A size-dependent model for predicting the mechanical behaviors of adhesively bonded layered structures based on strain gradient elasticity

Hao Long [a], Hansong Ma [b], Yueguang Wei [a,*], Yanwei Liu [a]

[a] *Department of Mechanics and Engineering Science, College of Engineering, BIC-ESAT, Peking University, Beijing 100871, China*
[b] *State Key Laboratory of Nonlinear Mechanics, Institute of Mechanics, Chinese Academy of Sciences, Beijing 100190, China*

ARTICLE INFO

ABSTRACT

As adhesively bonded layered devices scale down, micro-scale adhesive layers become common and play a key role in the overall performance of micro devices. Herein, we use the strain gradient elasticity to characterize the micro-scale adhesive layers and propose an analytical size-dependent model to predict the mechanical behaviors of adhesively bonded layered structures. The results indicate that the local interfacial tractions and the global adherend displacement both show strong size effects, especially for soft adhesives with low modulus. When the ratio of the adhesive layer thickness to its material characteristic length scale (on the order of microns), representing the scale of the layered structures, decreases to unity, the interfacial tractions increase substantially and the adherend displacement decreases significantly. Meanwhile, the adherend displacement is insensitive to the adhesive modulus. The present study reveals the stiffening behaviors of layered structures, which are attributed to the large strain gradients in the constrained micro-scale adhesive layers. The results can help us predict the deformation of adhesively bonded layered structures, and achieve high performance of micro devices by adhesive bonding.

1. Introduction

The bonding with adhesive layers has many advantages, such as the ability to join different materials, low mass density and low stress concentration [1,2]. Thus, the adhesive bonding technology has been widely used in layered devices, among which typical representatives are smart structures with piezoelectric actuators/sensors [3–5], flexible electronics [6,7] and micro-electromechanical systems (MEMS) [2,8]. The adhesive properties have been found to significantly affect the strain transfer between the host structures and the piezoelectric actuators/sensors [5,9]. In flexible electronics, the bonding by a thin layer of polydimethylsiloxane (PDMS) can yield strong interfaces between the silicon circuits and a wide range of substrates [10]. For three-dimensional MEMS integration and packaging, the adhesive wafer bonding is a crucial process [11]. Therefore, the adhesive layers play an important role in the overall performance of widely-used layered structures.

As the size of the layered structures is reduced, the adhesive layer thickness correspondingly decreases from macro to micro scale. Remarkably, when the adhesive layer thickness is on the order of hundred microns, the size effects of interfacial strength and fracture energy have been observed in many experiments [12–16]. For example, for the double cantilever beam (DCB) specimens with epoxy adhesives, Ji et al.

[12] showed that when the adhesive layer thickness decreases from 1 mm to 0.09 mm, the mode I interfacial strength increases while the fracture energy decreases. Similar trends were also observed in Li et al.'s experiments [13] on the scarf joints with silicone rubber adhesives, and they found that when the adhesive layer thickness is reduced to 0.1 mm, the interfacial tensile and shear strengths reach 2–5 times the adhesive bulk strengths. As the layered devices scale down, the micro-scale adhesive layers, deposited by spin-coating or other procedures, become common. For example, spin-casted silicone layers with a thickness of 10 μm were used to bond a stack of lead zirconate titanate (PZT) mechanical energy harvesters [17]. And a layer of liquid skin adhesive with a thickness of 3–4 μm was added to keep an electronic tattoo laminated on human skin [18]. When Park et al. [19] fabricated Si ribbons on plastic substrates, the thickness of the spin-coated epoxy adhesive layer is about one micron. The spin-coated adhesive layers with thicknesses of hundreds of nanometers can be seen in the adhesive wafer bonding for the integration of MEMS [2] and nano-electromechanical systems (NEMS) [20]. In many experiments, strong size effects of the mechanical behaviors in micro-scale metals [21,22] and polymers [23–25] have been observed. Thus, the mechanical behaviors of micro-scale adhesive layers (most are polymers) should also exhibit apparent size effects due to the increased importance of microstructure effects.

Nomenclature

a	distance from the plate end to the simple supports
b	width of the layered structure
E	Young's modulus
E_a	Young's modulus of the adhesive layer
E_b	Young's modulus of the host beam
E_p	Young's modulus of the bonded plate
f_i	body force vector
G_a	shear modulus of the adhesive layer
h_a	thickness of the adhesive layer
h_b	thickness of the host beam
h_p	thickness of the bonded plate
L	span length
L_p	plate length
l	material characteristic length scale
M_b	bending moment in the host beam
M_p	bending moment in the bonded plate
N_b	axial force in the host beam
N_p	axial force in the bonded plate
P	concentrated force
q	intensity of the distributed line load
r_i	double-stress traction vector
T_{ijklmn}	isotropic projection tensor
t_i	surface traction vector
u_a	displacement of the adhesive layer in the x direction
u_b	displacement of the host beam in the x direction
u_{b0}	displacement of the host beam at the middle plane in the x direction
u_i	displacement vector
u_p	displacement of the bonded plate in the x direction
u_{p0}	displacement of the bonded plate at the middle plane in the x direction
V_b	shear force in the host beam
V_p	shear force in the bonded plate
W	strain energy density (per unit volume)
w_a	displacement of the adhesive layer in the z direction
w_b	displacement of the host beam in the z direction (deflection)
w_M	midspan deflection of the host beam in layered structures
w_{M0}	midspan deflection of the host beam without a bonded plate
w_p	displacement of the bonded plate in the z direction (deflection)

Greek and special symbols

ε_{ij}	strain tensor
κ_{ijk}	strain gradient tensor
ν	Poisson's ratio
ν_a	Poisson's ratio of the adhesive layer
σ_{ij}	stress tensor
σ_{xxb}	axial stress in the host beam
σ_{xxp}	axial stress in the bonded plate
τ_{ijk}	high-order stress tensor
$(\hat{\cdot})$	dimensionless quantities
$(\bar{\cdot})$	dimensionless quantities divided by dimensionless force $(\hat{\cdot})/\bar{P}$
$\Delta \bar{u}$	difference of dimensionless axial displacements $\bar{u}_{b0} - \bar{u}_{p0}$

Considering the wide use of the micro-scale adhesive layers, how to characterize their size-dependent mechanical behaviors becomes essential. In order to predict the interfacial stresses and global displacements of layered structures with macro-scale adhesive layers, many re-

searchers adopted the shear-lag model [26,27] and the two-parameter elastic foundation model [28–30], where the latter considers the adhesive layer as continuously distributed tangential and normal springs. Nevertheless, these widely-used models are not applicable to describing the size-dependent behaviors of micro-scale adhesive layers, since they are within the framework of classical continuum mechanics, which is inherently scale-free. In contrast, size effects can be captured by the high-order continuum mechanics theories, which incorporate the intrinsic length scale parameters related to the microstructure, such as couple stress theories [31–33] and strain gradient theories [24,34–36]. On the basis of couple stress theories or strain gradient elasticity theories, many researchers investigated the size-dependent behaviors of layered structures, such as composite laminated beams [37,38], micro beams with piezoelectric actuators/sensors [39,40] and partially covered laminated micro beams [41]. However, these researchers mainly focused on the micro beams whose thicknesses are on the order of microns, and their models did not include the adhesive layers. To the best of our knowledge, Ascione's work [42] is one of the few studies which considered the size effects of micro-scale adhesives with high-order continuum mechanics theories, but the results were obtained from finite element simulations. Therefore, an analytical model accounting for the size effects of micro-scale adhesive layers is still lacking.

In a previous work [29], we studied the layered structures with macro-scale adhesive layers by the classical two-parameter elastic foundation model. Herein, we establish a size-dependent model of the layered structures with micro-scale or macro-scale adhesive layers, where the thin adhesive layer constrained between the adherends is characterized by strain gradient elasticity. This model can capture the size effects of the mechanical behaviors of layered structures, and is especially applicable to the layered structures with micro-scale adhesive layers.

The remainder of this paper is organized as follows. Section 2 presents the analytical formulation of the size-dependent model, including the governing equations and the solutions to displacements and interfacial tractions. The results of the size-dependent model for layered structures at different scales and the micro scale are respectively discussed in Section 3. Section 4 summarizes the main conclusions.

2. Analytical formulation of the size-dependent model

2.1. Problem statement

In micro devices, it is common to see host structures bonded with small-size piezoelectric actuators/sensors [4,43], and the substrate partially covered with inorganic electronic films [19]. Thus, the layered structure considered here consists of a host beam adhesively bonded by a partially covered plate (the plate length L_p is smaller than the span length L), as illustrated in Fig. 1. The layered structure with symmetrical geometry is subjected to three-point bending. However, we can extend the following analysis to the cases of more complicated geometry configurations and loading conditions. Hereafter, subscripts 'b', 'a' and 'p' refer to the host beam, the adhesive layer and the bonded plate, respectively. The thicknesses and the Young's moduli of the three layers are denoted by h_i and E_i (i = b, a, p), respectively. The Poisson's ratio of the adhesive layer is represented by ν_a.

The assumptions adopted in the present study are summarized as follows:

(1) The host beam, the adhesive layer and the bonded plate are isotropic and linearly elastic materials. The adhesive fracture and interface delamination are not considered.
(2) Only the mechanical behaviors of the plate are considered, and the electric-mechanical coupling behavior is not involved, since mechanical loads are inevitable whether for piezoelectric actuators/sensors or flexible electronics.
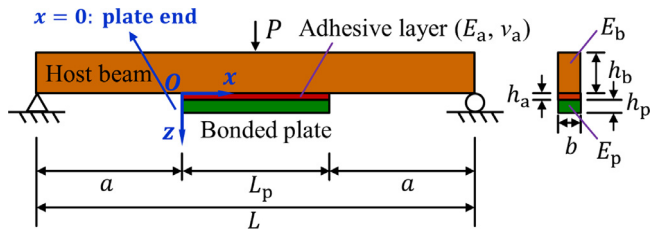
Fig. 1. Schematic diagram of the adhesively bonded layered structure under three-point bending. The plate length and the span length are denoted by L_p and L, respectively. And we have $L = L_p + 2a$, where a is the distance from the plate end to the simple supports. Parameters E and h represent Young's modulus and thickness, respectively, with subscripts 'b', 'a' and 'p' referring to the host beam, the adhesive layer and the bonded plate, respectively. The Poisson's ratio of the adhesive layer is denoted by v_a. All three layers have rectangle cross-sections with the same width (denoted by b). Under the Cartesian coordinate system shown above, the left end of the plate (or the adhesive layer) situates at $x = 0$ and the left end of the host beam situates at $x = -a$.

(3) The adherends, i.e., the host beam and the plate, are modeled by the classical Euler-Bernoulli beam theory, while the thin adhesive layer is characterized by the strain gradient elasticity. Similar to the classical analyses [28–30], the deformation of the adhesive layer is simplified as the combination of shear and tension/compression. Since the adhesive layer thickness is smaller than its length (i.e., $h_a \ll L_p$), and the adhesive layer modulus is also much smaller than those of the adherends, we only consider the strain gradient components along the adhesive thickness direction, referring to [50].

2.2. Governing equations

2.2.1. A brief review of the simplified strain gradient theory

The simplified strain gradient theory presented here is mostly within the framework of Mindlin's strain gradient elasticity theory [35], but the constitutive relations are directly obtained from Wei-Hutchinson strain gradient theory [44], where both the elastic and plastic strain gradients are considered. For solids in elastic deformation, Wei-Hutchinson strain gradient theory [44] has a simplified form [45,46], and it is introduced briefly as follows.

For a given displacement field u_i, the strain tensor ε_{ij} and the strain gradient tensor κ_{ijk} are defined respectively as

$$\varepsilon_{ij} = \frac{1}{2}\left(u_{i,j} + u_{j,i}\right), \; \kappa_{ijk} = \kappa_{jik} = u_{k,ij}. \tag{1}$$

The variation of the strain energy density (per unit volume) $W(\varepsilon_{ij}, \kappa_{ijk})$ gives

$$\delta W = \sigma_{ij}\delta\varepsilon_{ij} + \tau_{ijk}\delta\kappa_{ijk}, \tag{2}$$

where σ_{ij} is the stress tensor and τ_{ijk} is the high-order stress tensor. The stress tensor and the high-order stress tensor are expressed respectively as

$$\sigma_{ij} = \frac{\partial W}{\partial \varepsilon_{ij}}, \; \tau_{ijk} = \tau_{jik} = \frac{\partial W}{\partial \kappa_{ijk}}. \tag{3}$$

When the line loads along the surface edges are ignored, the principle of virtual work can be written as [35,47]

$$\int_V \left(\sigma_{ij}\delta\varepsilon_{ij} + \tau_{ijk}\delta\kappa_{ijk}\right)\mathrm{d}V = \int_V f_i\delta u_i\mathrm{d}V + \int_S t_i\delta u_i\mathrm{d}S + \int_S r_i D\left(\delta u_i\right)\mathrm{d}S, \tag{4}$$

where $\mathrm{d}V$ and $\mathrm{d}S$ are the volume and boundary area elements, f_i is the body force, t_i is the surface traction and r_i is the double-stress traction. On the boundary S, the gradient of displacements can be divided into two independent parts:

$$u_{i,j} = n_j D u_i + D_j u_i, \tag{5}$$

where $D = n_k \partial_k$ is the normal derivative operator and $D_j = \partial_j - n_j D$ is the surface-gradient operator.

From Eq. (4), we can obtain the equilibrium equations:

$$\sigma_{ik,i} - \tau_{ijk,ij} + f_k = 0, \tag{6}$$

and the boundary conditions:

$$t_k = n_i\left(\sigma_{ik} - \tau_{ijk,j}\right) + n_i n_j \tau_{ijk}\left(D_p n_p\right) - D_j\left(n_i \tau_{ijk}\right), \tag{7a}$$

$$r_k = n_i n_j \tau_{ijk}, \tag{7b}$$

where t_k is the surface traction and r_k is the double-stress traction.

For strain gradient elasticity, the simplified constitutive relations of Wei-Hutchinson strain gradient theory can be written as [46]

$$\sigma_{ij} = \frac{Ev}{(1+v)(1-2v)}\varepsilon_{kk}\delta_{ij} + \frac{E}{1+v}\varepsilon_{ij}, \tag{8a}$$

$$\tau_{ijk} = 2E\sum_{I=1}^{4}\left[l^{(I)}\right]^2 T^{(I)}_{ijklmn}\kappa_{lmn}, \tag{8b}$$

where E is the Young's modulus, v is the Poisson's ratio and $l^{(I)}$ are the material characteristic length scales, and $T^{(I)}_{ijklmn}$ are isotropic projection tensors (see Ref. [44]). When $l^{(I)} = l$ ($I = 1$–4), considering $\sum_{I=1}^{4} T^{(I)}_{ijklmn} = (\delta_{il}\delta_{jm} + \delta_{im}\delta_{jl})\delta_{kn}/2$, Eq. (8b) can be further simplified as [45]

$$\tau_{ijk} = 2El^2\kappa_{ijk}. \tag{9}$$

Although a simplified strain gradient elasticity theory involving only one non-classical parameter has also been proposed by Altan and Aifantis [34], its constitutive relations are different from the present ones.

2.2.2. Governing equations of the adhesive displacements and the interfacial tractions

The motivation for exploring the strain gradient effects in the constrained adhesive layers derives from the experiments about the interfacial strength of adhesively bonded layered structures. Previous experimental results [12,13,16] showed that the interfacial strength, dependent on the adhesive layer thickness, can reach several times the adhesive bulk strength when the adhesive layer thickness decreases to the order of hundred microns. For example, for the aluminum alloy/silicone rubber adhesive layer/aluminum alloy system, at the adhesive layer thickness of 0.1 mm, the average interfacial tensile and shear strengths (about 1.8 MPa [13]) are several times the adhesive bulk strengths (the tensile and shear strengths of the bulk silicon rubber are 0.33 MPa and 0.55 MPa, respectively [16]). When we further decrease the adhesive layer thickness (below a hundred microns), we expect that the interfacial strength measured in the experiments will be much higher, as Ji et al. [12] have pointed out. This phenomenon can hardly be explained by the classical continuum mechanics, and its explanation may require the application of the strain gradient theory, on the basis of which the peak separation tractions above 10 times the yield stress can be attained [44]. Thus, we use the strain gradient elasticity to characterize the thin adhesive layer, which leads to the results distinct from those of the classical model (e.g., adhesive displacements and interfacial tractions).

Under the Cartesian coordinate system shown in Fig. 1, the displacements of the adhesive layer in the x and z directions are $u_a(x,z)$ and $w_a(x,z)$, respectively. Similar to the classical two-parameter elastic foundation model [28] or the adhesive layer theory [48], the soft adhesive layer mainly undergoes shear and lateral tension/compression deformations, corresponding to the strain components ε_{31} and ε_{33}, respectively. From Eq. (1), the strain gradient components along the thickness direction include κ_{331} and κ_{333}. Thus, from Eqs. (8a) and (9), the nonzero stress and high-order stress components can be expressed by
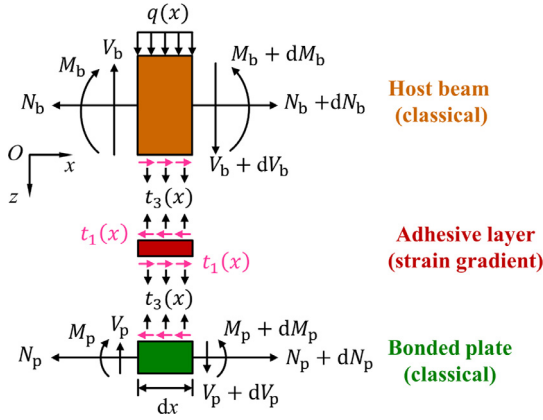
Fig. 2. Free-body diagram of an infinitesimal element with a length of dx in the adhesively bonded layered structure. We use parameters N, M, and V to denote axial force, bending moment and shear force, respectively, with subscripts 'b' and 'p' referring to the host beam and the bonded plate. The shear and normal tractions at the interfaces are $t_1(x)$ and $t_3(x)$, respectively. The intensity of the distributed line load is $q(x)$.

$$\sigma_{31} = 2G_a\varepsilon_{31}$$
$$= G_a\left(\frac{\partial u_a}{\partial z} + \frac{\partial w_a}{\partial x}\right),$$
$$\sigma_{33} = E_a\varepsilon_{33}$$
$$= E_a\frac{\partial w_a}{\partial z}, \tag{10a}$$

$$\tau_{331} = 2E_al^2\kappa_{331}$$
$$= 2E_al^2\frac{\partial^2 u_a}{\partial z^2},$$
$$\tau_{333} = 2E_al^2\kappa_{333}$$
$$= 2E_al^2\frac{\partial^2 w_a}{\partial z^2}, \tag{10b}$$

where $G_a = E_a/[2(1 + v_a)]$ is the shear modulus of the adhesive layer. If the high-order stresses are omitted, the strain gradient model degenerates into the classical model. The term $\partial w_a/\partial x$ in Eq. (10a) was neglected in some classical studies [28–30], but it is considered here for completeness, similar to [26,49]. If $w_a = 0$ and we only consider the shear deformation (ε_{31} and κ_{331}), the present model can degenerate into the strain gradient shear-lag model aimed at the staggered bio-structure materials [50].

From Eq. (6), the equilibrium equations in the adhesive layer are given by

$$\sigma_{31,3} - \tau_{331,33} = 0, \tag{11a}$$

$$\sigma_{33,3} - \tau_{333,33} = 0. \tag{11b}$$

Since the host beam and the bonded plate are characterized by classical elasticity, they cannot be subjected to the double-stress traction transferred from the interfaces. Thus, we only consider the transfer of surface tractions at the interfaces, as shown in Fig. 2. From Eq. (7a), the tractions at the interfaces ($z = 0$, h_a) are given by

$$t_1(x, z = 0) = (\sigma_{31} - \tau_{331,3})_{z=0}, \quad t_3(x, z = 0) = (\sigma_{33} - \tau_{333,3})_{z=0}, \tag{12a}$$

$$t_1(x, z = h_a) = (\sigma_{31} - \tau_{331,3})_{z=h_a}, \quad t_3(x, z = h_a) = (\sigma_{33} - \tau_{333,3})_{z=h_a}. \tag{12b}$$

From Eqs. (11), we can know that $\sigma_{31} - \tau_{331,3}$ and $\sigma_{33} - \tau_{333,3}$ are independent of z. Thus, the interfacial tractions at the upper and lower interfaces ($z = 0$, h_a) are equal, as shown in Fig. 2, and they can be written as

$$t_1(x, z = 0) = t_1(x, z = h_a) = \sigma_{31} - \tau_{331,3} = t_1(x), \tag{13a}$$

$$t_3(x, z = 0) = t_3(x, z = h_a) = \sigma_{33} - \tau_{333,3} = t_3(x). \tag{13b}$$

The equal interfacial tractions at the upper and lower interfaces directly result from the equilibrium of the adhesive layer. And this does not mean that the stress state is uniform across the adhesive layer thickness. Since we consider the strain gradient effects in the adhesive layer, the stress components (σ_{31}, σ_{33}) and the high-order stress components (τ_{331}, τ_{333}) vary with the coordinate z. Only their combinations $\sigma_{31} - \tau_{331,3}$ and $\sigma_{33} - \tau_{333,3}$ are independent of z, according to Eqs. (11).

Substitution of Eqs. (10) into Eqs. (11) gives

$$\frac{\partial^4 w_a}{\partial z^4} - \frac{1}{2l^2}\frac{\partial^2 w_a}{\partial z^2} = 0, \tag{14a}$$

$$\frac{\partial^4 u_a}{\partial z^4} - \frac{1}{4(1+v_a)l^2}\frac{\partial^2 u_a}{\partial z^2} = \frac{1}{4(1+v_a)l^2}\frac{\partial^2 w_a}{\partial x\partial z}. \tag{14b}$$

We assume that no work is done at the interfaces $z = 0$, h_a, and thus according to the virtual work principle Eq. (4), the displacement u_i and its normal gradient Du_i are continuous at the interfaces [50]. Therefore, we can obtain the following boundary conditions about w_a:

$$w_a(z = 0) = w_b, \quad \frac{\partial w_a}{\partial z}\Big|_{z=0} = \frac{\partial w_b}{\partial z}\Big|_{z=0} = 0, \tag{15a}$$

$$w_a(z = h_a) = w_p, \quad \frac{\partial w_a}{\partial z}\Big|_{z=h_a} = \frac{\partial w_p}{\partial z}\Big|_{z=h_a} = 0, \tag{15b}$$

where $w_b = w_b(x)$ and $w_p = w_p(x)$ are the deflections (displacements in the z direction) of the host beam and the bonded plate, respectively.

Similarly, the boundary conditions about u_a can also be obtained. Before that, we should give the adherend displacements from the classical Euler-Bernoulli beam theory:

$$u_b = u_{b0} - \left(z + \frac{h_b}{2}\right)\frac{dw_b}{dx}, \quad -h_b \le z < 0, \tag{16a}$$

$$u_p = u_{p0} - \left(z - \frac{h_p + 2h_a}{2}\right)\frac{dw_p}{dx}, \quad h_a \le z \le h_a + h_p, \tag{16b}$$

where u_b and u_p are the displacements of the host beam and the bonded plate in the x direction, respectively. At the middle planes, we have $u_b = u_{b0}$ for $z = -h_b/2$ and $u_p = u_{p0}$ for $z = h_a + h_p/2$. Therefore, the boundary conditions about u_a can be expressed by

$$u_a(z = 0) = u_b(z = 0) = u_{b0} - \frac{h_b}{2}\frac{dw_b}{dx}, \quad \frac{\partial u_a}{\partial z}\Big|_{z=0} = \frac{\partial u_b}{\partial z}\Big|_{z=0} = -\frac{dw_b}{dx}, \tag{17a}$$

$$u_a(z = h_a) = u_p(z = h_a) = u_{p0} + \frac{h_p}{2}\frac{dw_p}{dx}, \quad \frac{\partial u_a}{\partial z}\Big|_{z=h_a} = \frac{\partial u_p}{\partial z}\Big|_{z=h_a} = -\frac{dw_p}{dx}. \tag{17b}$$

If the dimensionless quantities are denoted by overlined letters, we have $\bar{x} = x/h_b$, $\bar{z} = z/h_a$, $\bar{w}_b = w_b/h_b$, $\bar{w}_a = w_a/h_b$, $\bar{w}_p = w_p/h_b$, $\bar{u}_{b0} = u_{b0}/h_b$, $\bar{u}_a = u_a/h_b$, $\bar{u}_{p0} = u_{p0}/h_b$, $\bar{h}_a = h_a/h_b$, $\bar{h}_p = h_p/h_b$, $\bar{t}_1 = t_1/E_b$, $\bar{t}_3 = t_3/E_b$, $\bar{E}_a = E_a/E_b$ and $\bar{G}_a = G_a/E_b$. Then, Eqs. (13)–(17) can be rewritten in a dimensionless form.

Solving Eqs. (14) in the dimensionless form, we can obtain the adhesive displacements as follows:

$$\bar{w}_a = C_1\cosh(\bar{A}\bar{z}) + C_2\sinh(\bar{A}\bar{z}) + C_3\bar{z} + C_4, \tag{18a}$$

$$\bar{u}_{\mathrm{a}} = \mathrm{C}_5 \cosh\left(\bar{B}\bar{z}\right) + \mathrm{C}_6 \sinh\left(\bar{B}\bar{z}\right) + \mathrm{C}_7 \bar{z} + \mathrm{C}_8 +$$

$$\frac{\bar{B}^2 \bar{h}_{\mathrm{a}}}{\left(\bar{A}^2 - \bar{B}^2\right)\bar{A}}\left(\frac{\mathrm{d}\bar{w}_{\mathrm{b}}}{\mathrm{d}\bar{x}} - \frac{\mathrm{d}\bar{w}_{\mathrm{p}}}{\mathrm{d}\bar{x}}\right)\left[a_{11}\sinh\left(\bar{A}\bar{z}\right) + a_{21}\cosh\left(\bar{A}\bar{z}\right)\right]$$
$$- \frac{a_{31}}{2\bar{h}_{\mathrm{a}}}\left(\frac{\mathrm{d}\bar{w}_{\mathrm{b}}}{\mathrm{d}\bar{x}} - \frac{\mathrm{d}\bar{w}_{\mathrm{p}}}{\mathrm{d}\bar{x}}\right)\bar{z}^2, \tag{18b}$$

where $\bar{A} = h_{\mathrm{a}}/(\sqrt{2}l)$, $\bar{B} = h_{\mathrm{a}}/(2l\sqrt{1+v_{\mathrm{a}}})$ and C_i $(i = 1–8)$ are integration constants determined by the boundary conditions of Eqs. (15) and (17):

$$\begin{pmatrix} \mathrm{C}_1 \\ \mathrm{C}_2 \\ \mathrm{C}_3 \\ \mathrm{C}_4 \end{pmatrix} = \begin{pmatrix} a_{11} & -a_{11} \\ a_{21} & -a_{21} \\ a_{31} & -a_{31} \\ 1-a_{11} & a_{11} \end{pmatrix} \begin{pmatrix} \bar{w}_{\mathrm{b}} \\ \bar{w}_{\mathrm{p}} \end{pmatrix}, \tag{19a}$$

$$\begin{pmatrix} \mathrm{C}_5 \\ \mathrm{C}_6 \\ \mathrm{C}_7 \\ \mathrm{C}_8 \end{pmatrix} = \begin{pmatrix} a_{51} & -a_{51} & a_{53} & a_{54} \\ a_{61} & -a_{61} & a_{63} & a_{64} \\ a_{71} & -a_{71} & a_{73} & a_{74} \\ 1-a_{51} & a_{51} & a_{83} & a_{84} \end{pmatrix} \begin{pmatrix} \bar{u}_{\mathrm{b}0} \\ \bar{u}_{\mathrm{p}0} \\ \frac{\mathrm{d}\bar{w}_{\mathrm{b}}}{\mathrm{d}\bar{x}} \\ \frac{\mathrm{d}\bar{w}_{\mathrm{p}}}{\mathrm{d}\bar{x}} \end{pmatrix}. \tag{19b}$$

The expressions of dimensionless coefficients a_{ij} are given in Appendix A.

Substituting Eqs. (10) and (18) into Eqs. (13), we can obtain the interfacial tractions:

$$\bar{t}_1 = \frac{\bar{G}_{\mathrm{a}}}{\bar{h}_{\mathrm{a}}}\left(a_{71}\Delta\bar{u} + \xi_1 \frac{\mathrm{d}\bar{w}_{\mathrm{b}}}{\mathrm{d}\bar{x}} + \xi_2 \frac{\mathrm{d}\bar{w}_{\mathrm{p}}}{\mathrm{d}\bar{x}}\right), \tag{20a}$$

$$\bar{t}_3 = a_{31}\frac{\bar{E}_{\mathrm{a}}}{\bar{h}_{\mathrm{a}}}\left(\bar{w}_{\mathrm{b}} - \bar{w}_{\mathrm{p}}\right), \tag{20b}$$

where $\Delta\bar{u} = \bar{u}_{\mathrm{b}0} - \bar{u}_{\mathrm{p}0}$, $\xi_1 = a_{73} + (1-a_{11})\bar{h}_{\mathrm{a}}$ and $\xi_2 = a_{74} + a_{11}\bar{h}_{\mathrm{a}}$. The interfacial tractions can be completely determined only when we obtain the displacements $\Delta\bar{u}$, $\bar{w}_{\mathrm{b}}$ and $\bar{w}_{\mathrm{p}}$, which will be given in the next section.

Although the governing equations of the deformation of the adhesive layer have been proposed, we should be concerned with the limitations of the present model. Firstly, as shown in Fig. 2, the moment equilibrium of the adhesive layer is not satisfied, similar to the classical analyses [28–30]. In this case, the adhesive layer mainly transfers forces rather than moments, and the strain gradient effects make the force transfer more efficient. When the adhesive layer thickness is small compared with the adherend thicknesses, the approximation of ignoring the moment equilibrium condition can always meet the accuracy requirements. Secondly, the free boundary conditions at the ends of the adhesive layer ($x = 0$, L_{p}, see Fig. 1) are not satisfied. It should be noted that this limitation also exists in the classical models [28–30], since the boundary conditions at some edges are hard to be taken into account in the one-dimensional (1D) analysis. However, the interfacial stresses obtained from the two-dimensional (2D) finite element method (FEM) [51] have shown close agreement with those of the classical analytical solutions [52], except in a narrow region near the plate end. In the present model, the strain gradients along the adhesive thickness direction, the dominated strain gradient components, are incorporated. Thus, we can think that the present model captures the key factors of the problem. Besides, we should also note that previous analytical solutions and finite element simulations [53,54] have revealed the boundary layers for the 1D strain gradient bars/beams. Therefore, possible boundary layer effects, corresponding to the boundary conditions at the adhesive ends, are ignored in the present model, and the results near there are inaccurate. For more accurate local results near the adhesive ends, we should resort to 2D FEM.

2.2.3. Governing equations of the adherend displacements

Since the layered structure is symmetrical about the midspan, as shown in Fig. 1, we only need to consider the left half of the structure. And the left half of the host beam can be divided into two parts: one part bonded with a plate ($0 \leq \bar{x} < \bar{L}_{\mathrm{p}}/2$, $\bar{L}_{\mathrm{p}} = L_{\mathrm{p}}/h_{\mathrm{b}}$), and the other part without a bonded plate ($-\bar{a} \leq \bar{x} < 0$, $\bar{a} = a/h_{\mathrm{b}}$).

When $0 \leq \bar{x} < \bar{L}_{\mathrm{p}}/2$, from Eqs. (16), axial stresses in the host beam and the plate can be obtained:

$$\sigma_{xx\mathrm{b}} = E_{\mathrm{b}}\frac{\partial u_{\mathrm{b}}}{\partial x} = E_{\mathrm{b}}\left[\frac{\mathrm{d}u_{\mathrm{b}0}}{\mathrm{d}x} - \left(z + \frac{h_{\mathrm{b}}}{2}\right)\frac{\mathrm{d}^2 w_{\mathrm{b}}}{\mathrm{d}x^2}\right], \tag{21a}$$

$$\sigma_{xx\mathrm{p}} = E_{\mathrm{p}}\frac{\partial u_{\mathrm{p}}}{\partial x} = E_{\mathrm{p}}\left[\frac{\mathrm{d}u_{\mathrm{p}0}}{\mathrm{d}x} - \left(z - \frac{h_{\mathrm{p}} + 2h_{\mathrm{a}}}{2}\right)\frac{\mathrm{d}^2 w_{\mathrm{p}}}{\mathrm{d}x^2}\right]. \tag{21b}$$

Then, the axial forces in the two layers are

$$N_{\mathrm{b}} = b\int_{-h_{\mathrm{b}}}^{0}\sigma_{xx\mathrm{b}}\mathrm{d}z = E_{\mathrm{b}}bh_{\mathrm{b}}\frac{\mathrm{d}u_{\mathrm{b}0}}{\mathrm{d}x}, \tag{22a}$$

$$N_{\mathrm{p}} = b\int_{h_{\mathrm{a}}}^{h_{\mathrm{a}}+h_{\mathrm{p}}}\sigma_{xx\mathrm{p}}\mathrm{d}z = E_{\mathrm{p}}bh_{\mathrm{p}}\frac{\mathrm{d}u_{\mathrm{p}0}}{\mathrm{d}x}. \tag{22b}$$

The bending moments about the respective middle planes can be expressed by

$$M_{\mathrm{b}} = b\int_{-h_{\mathrm{b}}}^{0}\sigma_{xx\mathrm{b}}\left(z + \frac{h_{\mathrm{b}}}{2}\right)\mathrm{d}z = -\frac{E_{\mathrm{b}}bh_{\mathrm{b}}^3}{12}\frac{\mathrm{d}^2 w_{\mathrm{b}}}{\mathrm{d}x^2}, \tag{23a}$$

$$M_{\mathrm{p}} = b\int_{h_{\mathrm{a}}}^{h_{\mathrm{a}}+h_{\mathrm{p}}}\sigma_{xx\mathrm{p}}\left(z - \frac{h_{\mathrm{p}} + 2h_{\mathrm{a}}}{2}\right)\mathrm{d}z = -\frac{E_{\mathrm{p}}bh_{\mathrm{p}}^3}{12}\frac{\mathrm{d}^2 w_{\mathrm{p}}}{\mathrm{d}x^2}. \tag{23b}$$

From Fig. 2, we can obtain the equilibrium equations of the host beam:

$$\frac{\mathrm{d}N_{\mathrm{b}}}{\mathrm{d}x} = -t_1(x)b, \tag{24a}$$

$$\frac{\mathrm{d}V_{\mathrm{b}}}{\mathrm{d}x} = -q(x) - t_3(x)b, \tag{24b}$$

$$\frac{\mathrm{d}M_{\mathrm{b}}}{\mathrm{d}x} = V_{\mathrm{b}} - t_1(x)b\frac{h_{\mathrm{b}}}{2}, \tag{24c}$$

Similarly, we can also obtain the equilibrium equations of the bonded plate:

$$\frac{\mathrm{d}N_{\mathrm{p}}}{\mathrm{d}x} = t_1(x)b, \tag{25a}$$

$$\frac{\mathrm{d}V_{\mathrm{p}}}{\mathrm{d}x} = t_3(x)b, \tag{25b}$$

$$\frac{\mathrm{d}M_{\mathrm{p}}}{\mathrm{d}x} = V_{\mathrm{p}} - t_1(x)b\frac{h_{\mathrm{p}}}{2}, \tag{25c}$$

where V_{b} and V_{p} are the shear forces in the host beam and plate, respectively. And $q(x)$ is the intensity of the distributed line load.

Substituting Eqs. (20), (22) and (23) into Eqs. (24) and (25) and reformulating them, we obtain the governing equations about displacements $u_{\mathrm{b}0}$, $u_{\mathrm{p}0}$, w_{b} and w_{p}:

$$\frac{\mathrm{d}^2\bar{u}_{\mathrm{b}0}}{\mathrm{d}\bar{x}^2} + \bar{E}_{\mathrm{p}}\bar{h}_{\mathrm{p}}\frac{\mathrm{d}^2\bar{u}_{\mathrm{p}0}}{\mathrm{d}\bar{x}^2} = 0, \tag{26a}$$

$$\xi_1\frac{\mathrm{d}\bar{w}_{\mathrm{b}}}{\mathrm{d}\bar{x}} + \xi_2\frac{\mathrm{d}\bar{w}_{\mathrm{p}}}{\mathrm{d}\bar{x}} = -\lambda_1\frac{\mathrm{d}^2\Delta\bar{u}}{\mathrm{d}\bar{x}^2} - a_{71}\Delta\bar{u}, \tag{26b}$$

$$\frac{\mathrm{d}^4\bar{w}_{\mathrm{b}}}{\mathrm{d}\bar{x}^4} - 12\frac{\bar{E}_{\mathrm{a}}}{\bar{h}_{\mathrm{a}}}a_{31}\left(\bar{w}_{\mathrm{b}} - \bar{w}_{\mathrm{p}}\right) + \lambda_2\frac{\mathrm{d}^3\Delta\bar{u}}{\mathrm{d}\bar{x}^3} = 12\bar{q}(\bar{x}), \tag{26c}$$

$$\lambda_3\frac{\mathrm{d}^4\bar{w}_{\mathrm{p}}}{\mathrm{d}\bar{x}^4} = -\lambda_1\frac{\mathrm{d}^5\Delta\bar{u}}{\mathrm{d}\bar{x}^5} - a_{71}\frac{\mathrm{d}^3\Delta\bar{u}}{\mathrm{d}\bar{x}^3} + \xi_1\lambda_2\left(1 + \bar{h}_{\mathrm{p}}\right)\frac{\mathrm{d}^3\Delta\bar{u}}{\mathrm{d}\bar{x}^3} - 12\xi_1\bar{q}(\bar{x}), \tag{26d}$$

with $\bar{E}_p = E_p/E_b$, $\bar{q} = q/(E_b b)$ and the parameters defined as

$$\lambda_1 = \frac{\bar{E}_p \bar{h}_p \bar{h}_a}{\left(1 + \bar{E}_p \bar{h}_p\right) \bar{G}_a}, \quad \lambda_2 = \frac{6 \bar{E}_p \bar{h}_p}{1 + \bar{E}_p \bar{h}_p}, \tag{27a}$$

$$\lambda_3 = \xi_2 - \bar{E}_p \bar{h}_p^3 \xi_1 = \frac{\bar{B} \sinh \bar{B}}{2 K_2} \left[\left(\bar{h}_p + \bar{h}_a\right) - \bar{E}_p \bar{h}_p^3 \left(1 + \bar{h}_a\right) \right], \tag{27b}$$

where K_2 is expressed by Eq. (A.4). According as whether the coefficient λ_3 in Eq. (26d) is zero or not, two cases should be discussed separately: the balanced case ($\lambda_3 = 0$) and the unbalanced case ($\lambda_3 \neq 0$). From Eq. (27b), the balanced case ($\lambda_3 = 0$) indicates a balanced state of the geometry and material parameters, and it includes the special case of identical moduli and thicknesses for the adherends, i.e., $\bar{E}_p = 1$ and $\bar{h}_p = 1$. In the balanced case, Eq. (26d) reduces to a five-order linear ordinary differential equation (ODE) about $\Delta \bar{u}$. While in the unbalanced case, $\Delta \bar{u}$ and $\bar{w}_p$ are coupled in Eq. (26d). The detailed discussions will be given in Section 2.3. If $\bar{h}_a \ll 1$ and $\bar{h}_a \ll \bar{h}_p$, the balanced case is reduced to $\bar{E}_p \bar{h}_p^2 = 1$, which is consistent with the classical studies [29,55].

When $-\bar{a} \leq \bar{x} < 0$, the governing equation of the host beam deflection is

$$\frac{d \bar{V}_b}{d \bar{x}} = -\frac{1}{12} \frac{d^4 \bar{w}_b}{d \bar{x}^4} = 0. \tag{28}$$

In order to give the boundary conditions, we should firstly express the internal forces in terms of displacements. From Eqs. (22)–(25), the dimensionless axial forces, bending moments and shear forces in the host beam and the bonded plate can be expressed by

$$\bar{N}_b = \frac{N_b}{b h_b E_b} = \frac{d \bar{u}_{b0}}{d \bar{x}}, \quad \bar{N}_p = \frac{N_p}{b h_b E_b} = \bar{E}_p \bar{h}_p \frac{d \bar{u}_{p0}}{d \bar{x}}, \tag{29a}$$

$$\bar{M}_b = \frac{M_b}{b h_b^2 E_b} = -\frac{1}{12} \frac{d^2 \bar{w}_b}{d \bar{x}^2}, \quad \bar{M}_p = \frac{M_p}{b h_b^2 E_b} = -\frac{\bar{E}_p \bar{h}_p^3}{12} \frac{d^2 \bar{w}_p}{d \bar{x}^2}, \tag{29b}$$

$$\bar{V}_b = \frac{V_b}{b h_b E_b} = -\frac{1}{12} \frac{d^3 \bar{w}_b}{d \bar{x}^3} + \frac{1}{2} \bar{t}_1(\bar{x}), \quad \bar{V}_p = \frac{V_p}{b h_b E_b} = -\frac{\bar{E}_p \bar{h}_p^3}{12} \frac{d^3 \bar{w}_p}{d \bar{x}^3}$$
$$+ \frac{\bar{h}_p}{2} \bar{t}_1(\bar{x}). \tag{29c}$$

Equations (29) are also valid for $-\bar{a} \leq \bar{x} < 0$ since $\bar{t}_1(\bar{x}) = 0$.

The boundary conditions are proposed as follows. At the simple supports ($x = -a$), the deflection and the bending moment are zero, i.e.,

$$\bar{w}_b(\bar{x} = -\bar{a}) = 0, \quad \frac{d^2 \bar{w}_b}{d \bar{x}^2} \Big|_{\bar{x}=-\bar{a}} = 0. \tag{30}$$

At the plate end ($x = 0$), the axial forces in the host beam and the plate are zero. The deflection, the slope, the bending moment and the shear force in the host beam are continuous. Besides, the bending moment and the shear force in the plate are zero. From Eqs. (29), these conditions yield

$$\frac{d \bar{u}_{b0}}{d \bar{x}} \Big|_{\bar{x}=0} = 0, \quad \frac{d \bar{u}_{p0}}{d \bar{x}} \Big|_{\bar{x}=0} = 0, \tag{31a}$$

$$\bar{w}_b(\bar{x} = 0^-) = \bar{w}_b(\bar{x} = 0^+), \quad \frac{d \bar{w}_b}{d \bar{x}} \Big|_{\bar{x}=0^-} = \frac{d \bar{w}_b}{d \bar{x}} \Big|_{\bar{x}=0^+}, \tag{31b}$$

$$\frac{d^2 \bar{w}_b}{d \bar{x}^2} \Big|_{\bar{x}=0^-} = \frac{d^2 \bar{w}_b}{d \bar{x}^2} \Big|_{\bar{x}=0^+}, \quad \frac{d^3 \bar{w}_b}{d \bar{x}^3} \Big|_{\bar{x}=0^-} = \frac{d^3 \bar{w}_b}{d \bar{x}^3} \Big|_{\bar{x}=0^+} - 6 \bar{t}_1(0), \tag{31c}$$

$$\frac{d^2 \bar{w}_p}{d \bar{x}^2} \Big|_{\bar{x}=0} = 0, \quad \bar{E}_p \bar{h}_p^2 \frac{d^3 \bar{w}_p}{d \bar{x}^3} \Big|_{\bar{x}=0} - 6 \bar{t}_1(0) = 0. \tag{31d}$$

At the midspan ($x = L_p/2$), the axial displacements and slopes in the host beam and the plate are zero. The dimensionless shear force in the host beam is $\bar{V}_b = \bar{P}/2$, where $\bar{P} = P/(E_b b h_b)$, and the shear force in the plate is zero. From Eqs. (29), these conditions can be expressed by

$$\bar{u}_{b0} \left(\frac{\bar{L}_p}{2} \right) = 0, \quad \bar{u}_{p0} \left(\frac{\bar{L}_p}{2} \right) = 0, \tag{32a}$$

$$\frac{d \bar{w}_b}{d \bar{x}} \Big|_{\bar{x}=\bar{L}_p/2} = 0, \quad \frac{d \bar{w}_p}{d \bar{x}} \Big|_{\bar{x}=\bar{L}_p/2} = 0, \tag{32b}$$

$$\frac{d^3 \bar{w}_b}{d \bar{x}^3} \Big|_{\bar{x}=\bar{L}_p/2} = -6 \bar{P}, \quad \frac{d^3 \bar{w}_p}{d \bar{x}^3} \Big|_{\bar{x}=\bar{L}_p/2} = 0. \tag{32c}$$

2.3. Solutions to displacements and interface tractions

2.3.1. Balanced case

For the balanced case ($\lambda_3 = 0$), considering $\bar{q}(\bar{x}) = 0$ for three-point bending, Eq. (26d) reduces to a five-order linear ODE:

$$\frac{d^5 \Delta \bar{u}}{d \bar{x}^5} - m_1^2 \frac{d^3 \Delta \bar{u}}{d \bar{x}^3} = 0, \tag{33}$$

where m_1 is the parameter defined by

$$m_1^2 = \frac{\bar{G}_a \bar{B} \sinh \bar{B}}{\bar{h}_a K_2} \left[1 + \frac{1}{\bar{E}_p \bar{h}_p} + 3\left(1 + \bar{h}_p\right)\left(1 + \bar{h}_a\right) \right] > 0. \tag{34}$$

Solving Eq. (33), we can obtain

$$\Delta \bar{\bar{u}} = D_1 \cosh\left(m_1 \bar{x}\right) + D_2 \sinh\left(m_1 \bar{x}\right) + D_3 \bar{x}^2 + D_4 \bar{x} + D_5, \tag{35}$$

where $\Delta \bar{\bar{u}} = \Delta \bar{u}/\bar{P}$. In Eq. (35) and the following equations, $D_j(j = 1$–14) are integration constants.

From Eqs. (26b), 26c) and ((35), we have

$$\frac{d^5 \bar{\bar{w}}_b}{d \bar{x}^5} + 4 m_2^4 \frac{d \bar{\bar{w}}_b}{d \bar{x}} = m_3 \left[D_1 \cosh\left(m_1 \bar{x}\right) + D_2 \sinh\left(m_1 \bar{x}\right) \right]$$
$$+ m_4 \left(D_3 \bar{x}^2 + D_4 \bar{x} \right) + m_5, \tag{36}$$

where $\bar{\bar{w}}_b = \bar{w}_b/\bar{P}$ and

$$m_2^4 = -\frac{3\left(1 + \bar{E}_p \bar{h}_p^3\right)}{\bar{E}_p \bar{h}_p^3} \frac{\bar{E}_a}{\bar{h}_a} a_{31} > 0, \quad m_3 = -\lambda_2 m_1^4 + \frac{72 \bar{E}_a \left(1 + \bar{h}_p\right) a_{31}}{\bar{h}_a \left(1 + \bar{E}_p \bar{h}_p\right) \bar{h}_p^2}, \tag{37a}$$

$$m_4 = \frac{12 \bar{E}_a a_{31} a_{71}}{\bar{h}_a \xi_2}, \quad m_5 = \frac{24 \bar{E}_p \bar{h}_p \bar{E}_a a_{31}}{\left(1 + \bar{E}_p \bar{h}_p\right) \xi_2 \bar{G}_a} D_3 + m_4 D_5. \tag{37b}$$

Solving Eq. (36), we can obtain

$$\bar{\bar{w}}_b = \cosh\left(m_2 \bar{x}\right) \left[D_6 \cos\left(m_2 \bar{x}\right) + D_7 \sin\left(m_2 \bar{x}\right) \right] +$$

$$\sinh\left(m_2 \bar{x}\right) \left[D_8 \cos\left(m_2 \bar{x}\right) + D_9 \sin\left(m_2 \bar{x}\right) \right] +$$

$$\frac{m_3}{\left(m_1^4 + 4 m_2^4\right) m_1} \left[D_2 \cosh\left(m_1 \bar{x}\right) + D_1 \sinh\left(m_1 \bar{x}\right) \right] +$$

$$\frac{m_4}{12 m_2^4} D_3 \bar{x}^3 + \frac{m_4}{8 m_2^4} D_4 \bar{x}^2 + \frac{m_5}{4 m_2^4} \bar{x} + D_{10}, 0 \leq \bar{x} < \bar{L}_p/2. \tag{38}$$

From Eq. (26c), the deflection of the plate $\bar{\bar{w}}_b = \bar{w}_p/\bar{P}$ is given by

$$\bar{\bar{w}}_p = \bar{\bar{w}}_b - \frac{\bar{h}_a}{12 \bar{E}_a a_{31}} \left(\frac{d^4 \bar{\bar{w}}_b}{d \bar{x}^4} + \lambda_2 \frac{d^3 \Delta \bar{\bar{u}}}{d \bar{x}^3} \right), 0 \leq \bar{x} < \bar{L}_p/2. \tag{39}$$

From Eqs. (26a) and (35), the axial displacements in the host beam and the plate can be expressed by

$$\bar{\bar{u}}_{b0} = \frac{1}{1 + \bar{E}_p \bar{h}_p} \left(\bar{E}_p \bar{h}_p \Delta \bar{\bar{u}} + D_{11} \bar{x} + D_{12} \right), 0 \leq \bar{x} < \bar{L}_p/2, \tag{40a}$$

$$\bar{\bar{u}}_{p0} = \frac{1}{1 + \bar{E}_p \bar{h}_p} \left(-\Delta \bar{\bar{u}} + D_{11} \bar{x} + D_{12} \right), 0 \leq \bar{x} < \bar{L}_p/2, \tag{40b}$$

where $\bar{\bar{u}}_{b0} = \bar{u}_{b0}/\bar{P}$ and $\bar{\bar{u}}_{p0} = \bar{u}_{p0}/\bar{P}$.

For the part of the host beam not bonded with a plate, its deflection can be obtained from Eqs. (28) and (30):

$$\bar{\bar{w}}_b = D_{13}(\bar{x} + \bar{a})^3 + D_{14}(\bar{x} + \bar{a}), -\bar{a} \leq \bar{x} < 0. \tag{41}$$

At this moment, the solutions of all displacements have been obtained, i.e., Eqs. (38)–(41), where the integration constants $D_j(j = 1$–14) can be determined by the boundary conditions (i.e., Eqs. (31) and (32)). Then, the interfacial tractions can be obtained by substitution of Eqs. (35), (38) and (39) into Eqs. (20).

2.3.2. Unbalanced case

For the unbalanced case ($\lambda_3 \neq 0$), we need to solve Eqs. (26) simultaneously to obtain all the displacements. From Eqs. (26b)–(26d), we can obtain the following nine-order linear ODE ($\bar{q}(\bar{x}) = 0$ for three-point bending):

$$\frac{d^9 \Delta \bar{\bar{u}}}{d\bar{x}^9} - \alpha_1 \frac{d^7 \Delta \bar{\bar{u}}}{d\bar{x}^7} + \alpha_2 \frac{d^5 \Delta \bar{\bar{u}}}{d\bar{x}^5} - \alpha_3 \frac{d^3 \Delta \bar{\bar{u}}}{d\bar{x}^3} = 0, \tag{42}$$

where $\alpha_j (j = 1\text{–}3)$ are positive parameters defined as

$$\alpha_1 = \frac{\bar{G}_a}{\bar{h}_a \bar{E}_p \bar{h}_p^2} \left[6 \left(\xi_2 + \bar{E}_p \bar{h}_p^2 \xi_1 \right) - a_{71} \bar{h}_p \left(1 + \bar{E}_p \bar{h}_p \right) \right], \tag{43a}$$

$$\alpha_2 = -\frac{12 \bar{E}_a a_{31}}{\bar{h}_a} \left(1 + \frac{1}{\bar{E}_p \bar{h}_p^3} \right), \tag{43b}$$

$$\alpha_3 = -\frac{12 \bar{E}_a \bar{G}_a a_{31}}{\bar{h}_a^2 \bar{E}_p^2 \bar{h}_p^4} \left[6 \bar{E}_p \bar{h}_p \left(1 + \bar{h}_p \right) \left(\xi_1 + \xi_2 \right) - \left(1 + \bar{E}_p \bar{h}_p \right) \left(1 + \bar{E}_p \bar{h}_p^3 \right) a_{71} \right]. \tag{43c}$$

For typical material and geometry parameters, the characteristic equation of Eq. (42) has two nonzero real roots, two pairs of conjugate complex roots and three zero roots (see Appendix B). Thus, the solution of Eq. (42) can be expressed by

$$\Delta \bar{\bar{u}} = D_1 \cosh\left(\eta_1 \bar{x} \right) + D_2 \sinh\left(\eta_1 \bar{x} \right) + \cosh\left(\gamma_1 \bar{x} \right) \left[D_3 \cos\left(\gamma_2 \bar{x} \right) + D_4 \sin\left(\gamma_2 \bar{x} \right) \right] +$$

$$\sinh\left(\gamma_1 \bar{x} \right) \left[D_5 \cos\left(\gamma_2 \bar{x} \right) + D_6 \sin\left(\gamma_2 \bar{x} \right) \right] + D_7 \bar{x}^2 + D_8 \bar{x} + D_9, \tag{44}$$

where η_1, γ_1 and γ_2 are positive parameters given by Eqs. (B.6) and (B.7).

Afterwards, from Eqs. (26b)–(26d), we can obtain the deflections of the host beam and the bonded plate for $0 \leq \bar{x} < \bar{L}_p/2$:

$$\bar{w}_b = -\frac{\lambda_1}{\xi_1 + \xi_2} \frac{d\Delta \bar{\bar{u}}}{d\bar{x}} - \frac{a_{71}}{\xi_1 + \xi_2} \int_0^{\bar{x}} \Delta \bar{\bar{u}} \, d\bar{x} + \alpha_4 \left(\frac{d^5 \Delta \bar{\bar{u}}}{d\bar{x}^5} - \alpha_1 \frac{d^3 \Delta \bar{\bar{u}}}{d\bar{x}^3} \right) + D_{10}, \tag{45}$$

$$\bar{w}_p = -\frac{\lambda_1}{\xi_1 + \xi_2} \frac{d\Delta \bar{\bar{u}}}{d\bar{x}} - \frac{a_{71}}{\xi_1 + \xi_2} \int_0^{\bar{x}} \Delta \bar{\bar{u}} \, d\bar{x} - \alpha_4 \left(\frac{d^5 \Delta \bar{\bar{u}}}{d\bar{x}^5} - \alpha_1 \frac{d^3 \Delta \bar{\bar{u}}}{d\bar{x}^3} \right) + D_{10}, \tag{46}$$

with parameter α_4 defined as

$$\alpha_4 = \frac{\bar{E}_p^2 \bar{h}_p^4 \bar{h}_a^2 \xi_2}{12 \left(1 + \bar{E}_p \bar{h}_p \right) \left(\xi_1 + \xi_2 \right) a_{31} \lambda_3 \bar{G}_a \bar{E}_a}. \tag{47}$$

For the unbalanced case, Eqs. (40) and (41) are also valid, but the expression of $\Delta \bar{\bar{u}}$ is different. Substituting Eq. (44) into Eqs. (40), (45) and (46), we can obtain the solutions of all displacements, and the integration constants $D_j (j = 1\text{–}14)$ can be determined by the boundary conditions (i.e., Eqs. (31) and (32)). Then, the interfacial tractions can be obtained by substitution of Eqs. (44)–(46) into Eqs. (20).

3. Results and discussions

In this section, we focus on the solutions of the local interfacial tractions and the global host beam deflection. And referring to previous literature, we can take typical values of the geometry and material parameters. For aluminum beams bonded with PZT actuators [56], the adhesive layer thickness varies from 20 μm to 1 mm. And we have $E_p = E_b = 70$ GPa, $E_a = 3$ GPa, $\nu_a = 0.4$, $h_p = 1$ mm and $h_b = 1\text{–}100$ mm. In flexible electronics [19], Si ribbons with thickness varying from 100 nm to 10 μm are bonded to a poly(ethyleneterepthalate) (PET) substrate (50 μm or 175 μm thick) with a thin epoxy adhesive layer (about 1 μm thick). The Young's moduli of the Si ribbons and the substrate are 130 GPa and 4 GPa, respectively. The Young's modulus

and Poisson's ratio of the adhesive layer are 4.4 GPa and 0.44, respectively. Besides, the adhesive layer can be very soft. For example, the Young's modulus of silicone layers (adhesives, $E_a = 60$ kPa) is about five orders of magnitude smaller than that of the polyimide layers (adherends, $E = 2.5$ GPa) [57]. Considering these facts, the ranges of parameters in the following discussions are $h_a/l = 0.1\text{–}100$, $h_a/h_b = 10^{-2}$, $h_p/h_b = 0.1\text{–}1$, $L_p/L = 0.01\text{–}1$, $L/h_b = 20$, $E_a/E_b = 10^{-5}\text{–}10^{-1}$, $\nu_a = 0.4$ and $E_p/E_b = 0.1\text{–}50$. In the strain gradient theories, the material characteristic length scale is always on the order of microns ($l = 0.1\text{–}10 \, \mu$m) [21,24,45,58]. Thus, typically, for $l \approx 1 \, \mu$m, the host beam thickness is $h_b \approx 100 \, \mu$m and the minimum plate thickness is $h_p \approx 10 \, \mu$m.

In the following discussions, we will firstly compare the strain gradient solutions of layered structures at different scales, which will degenerate into the classical solution for the macro scale. Then, we will focus on the layered structures at the micro scale (with micro-scale adhesives). Here, since the geometry parameters span several orders (e.g., $h_a/h_b = 10^{-2}$), we use the adhesive layer thickness, the smallest geometry parameter, to represent the scale of the layered structure.

3.1. Results of adhesively bonded layered structures at different scales

3.1.1. Distributions of interfacial tractions

From the strain gradient model, the dimensionless interfacial tractions can be expressed as

$$\frac{t_i b h_b}{P} = f_i \left(\underbrace{\frac{x}{L_p}, \frac{h_a}{l}}_{\text{scale}}, \underbrace{\frac{h_a}{h_b}, \frac{h_p}{h_b}, \frac{L_p}{L}, \frac{L}{h_b}}_{\text{geometry}}, \underbrace{\frac{E_a}{E_b}, \nu_a, \frac{E_p}{E_b}}_{\text{material}} \right), \quad i = 1, 3. \tag{48}$$

As illustrated in Fig. 3, for adhesively bonded layered structures with similar geometry and material properties (i.e., the geometry and material parameters in Eq. (48) are identical), the parameter h_a/l characterizes the structure scale (including the scale of the adhesive layer). When h_a/l increases from 10^{-3} to 10^3 (l is a micron-scale parameter), the order of the adhesive layer thickness varies from nanometers to millimeters. Correspondingly, the geometry parameters vary in equal proportion. When h_a/l tends to infinity, Eq. (48) degenerates into the classical solution. It should be noted that from the classical solution, the dimensionless interfacial tractions are the same for similar geometry and material properties, regardless of the structure scales.

Distributions of interfacial tractions (i.e., interfacial stresses, $t_i = \sigma_{3i} (i = 1, 3)$) for layered structures at the macro scale, obtained from the classical solution, are shown in Fig. 4. Similar classical results have been presented by Long et al. [29], but they ignored the term $\partial w_a / \partial x$ in Eq. (10a) for small thickness ratios of adhesive layer to adherends. We can also obtain an approximate strain gradient solution by ignoring this term in Eq. (10a) (see Appendix C). From Fig. 4(a), the shear traction reaches its maximum at the plate end, and then decreases to zero at the midspan due to its antisymmetry distribution. From Fig. 4(b), high tensile traction occurs at the plate end, and the normal traction decays to zero somewhere far away from the plate end. And a compression zone can be observed next to the tension zone, which is reasonable considering that the resultant force of the normal traction is zero. Actually, we have $\int_0^{\bar{L}_p/2} \bar{t}_3(\bar{x}) d\bar{x} = \bar{V}_p(\bar{L}_p/2) - \bar{V}_p(0) = 0$ from Eq. (25b), indicating the force equilibrium in the z direction for the plate. Influences of dimensionless adhesive layer thickness h_a/h_b, a geometry parameter, are also shown in Fig. 4. With the decrease of h_a/h_b, interfacial shear and normal tractions increase in a wide region of the interface. The previous study [51] has shown that the approximate analytical solutions [52] are in good agreement with the results of FEM, except in a narrow region near the plate end (approximately $x/L_p \leq 0.1\%$).

Distributions of interfacial tractions for layered structures at different scales (represented by h_a/l) are shown in Fig. 5. All these results
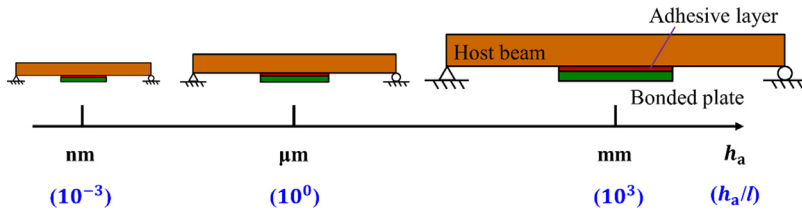
Fig. 3. Schematic diagram of adhesively bonded layered structures with similar geometry and material properties at different scales. The structure scale can be represented by the parameter h_a/l, where h_a is the adhesive layer thickness and l is the material characteristic length scale of the adhesive (l is a micron-scale parameter).
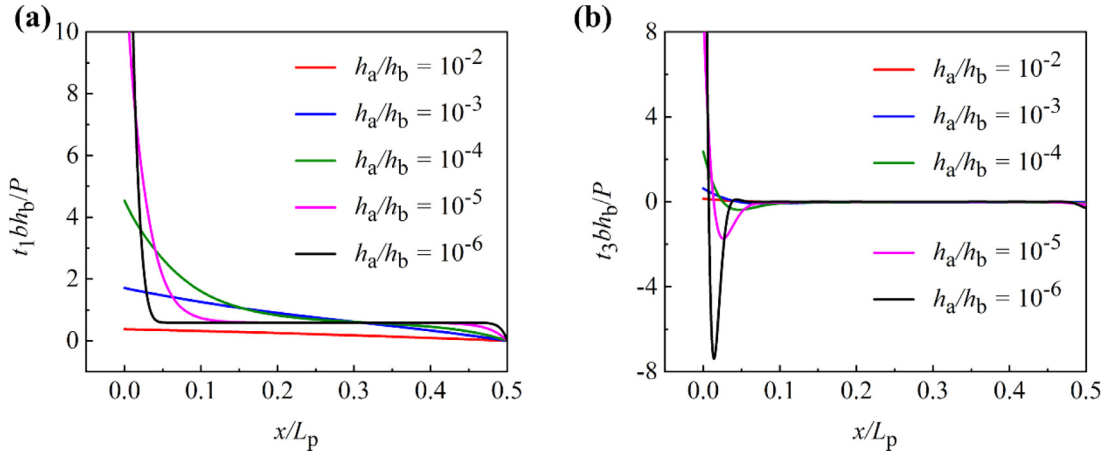
Fig. 4. Distributions of interfacial tractions for layered structures at the macro scale (obtained from the classical solution) for different values of dimensionless adhesive layer thickness h_a/h_b: dimensionless (a) interfacial shear traction $t_1 b h_b/P$ and (b) interfacial normal traction $t_3 b h_b/P$ versus normalized distance from the plate end x/L_p. The values of other parameters are fixed at $h_p/h_b = 0.1$, $L_p/L = 0.5$, $L/h_b = 20$, $E_a/E_b = 10^{-4}$, $v_a = 0.4$ and $E_p/E_b = 10$.
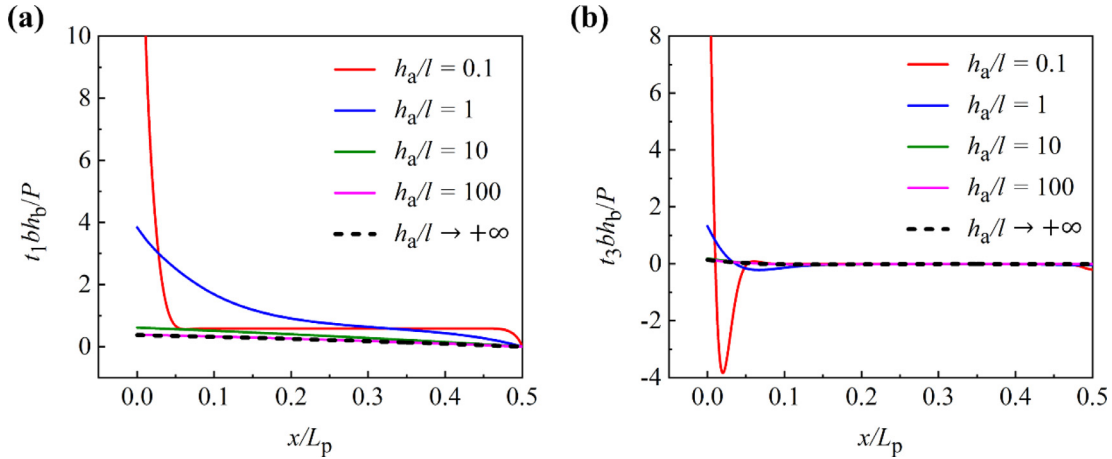
Fig. 5. Distributions of interfacial tractions for layered structures at different scales (represented by h_a/l): dimensionless (a) interfacial shear traction $t_1 b h_b/P$ and (b) interfacial normal traction $t_3 b h_b/P$ versus normalized distance from the plate end x/L_p. The values of other parameters are fixed at $h_a/h_b = 10^{-2}$, $h_p/h_b = 0.1$, $L_p/L = 0.5$, $L/h_b = 20$, $E_a/E_b = 10^{-4}$, $v_a = 0.4$ and $E_p/E_b = 10$. The limiting case of $h_a/l \to +\infty$ (dashed curves) corresponds to the classical solution.

correspond to the unbalanced case ($\lambda_3 \neq 0$ from Eq. (27b)). The importance of the strain gradient solution (solid lines) can be seen by comparing it with the classical solution (dashed lines). As mentioned before, the parameter h_a/l characterizes the structure scale. From Fig. 5, with the decrease of h_a/l, the strain gradient solution deviates more significantly from the classical solution. Moreover, the interfacial shear and normal tractions increase in a relatively wide region of the interface, since the constrained adhesive layer undergoes obvious nonuniform deformation and large strain gradients exist. Therefore, the interfacial tractions show an apparent size effect when the layered structure scales down (h_a/l decreases). It is noteworthy that when $h_a/l = 1$ (correspondingly, the adhesive layer thickness is $h_a = 0.1–10 \ \mu$m), the interfacial tractions increase substantially, indicating the stiff interface bonding created by the micro-scale adhesive layers. It should be noted that the results in a

narrow region near the plate end ($x/L_p \to 0$) are inaccurate since we ignore the boundary conditions near the adhesive ends. Previous experiments [13] have shown that the average interfacial tensile and shear strengths are several times the adhesive bulk strengths when h_a is about 100 μm, and the local strength should be much higher. Thus, the experimental results provide qualitative evidence for high interfacial tractions predicted by our model.

Although the increased interfacial tractions with varying parameter are both observed in Figs. 4 and 5, the underlying reasons are totally different. In Fig. 4, the variation of interfacial tractions with thickness ratio h_a/h_b shows geometry effects for layered structures at the macro scale ($h_a/l \to +\infty$). In contrast, in Fig. 5, the variation of interfacial tractions with structure scale h_a/l for fixed h_a/h_b reflects the size effects for layered structures at different scales (correspondingly, the adhesive
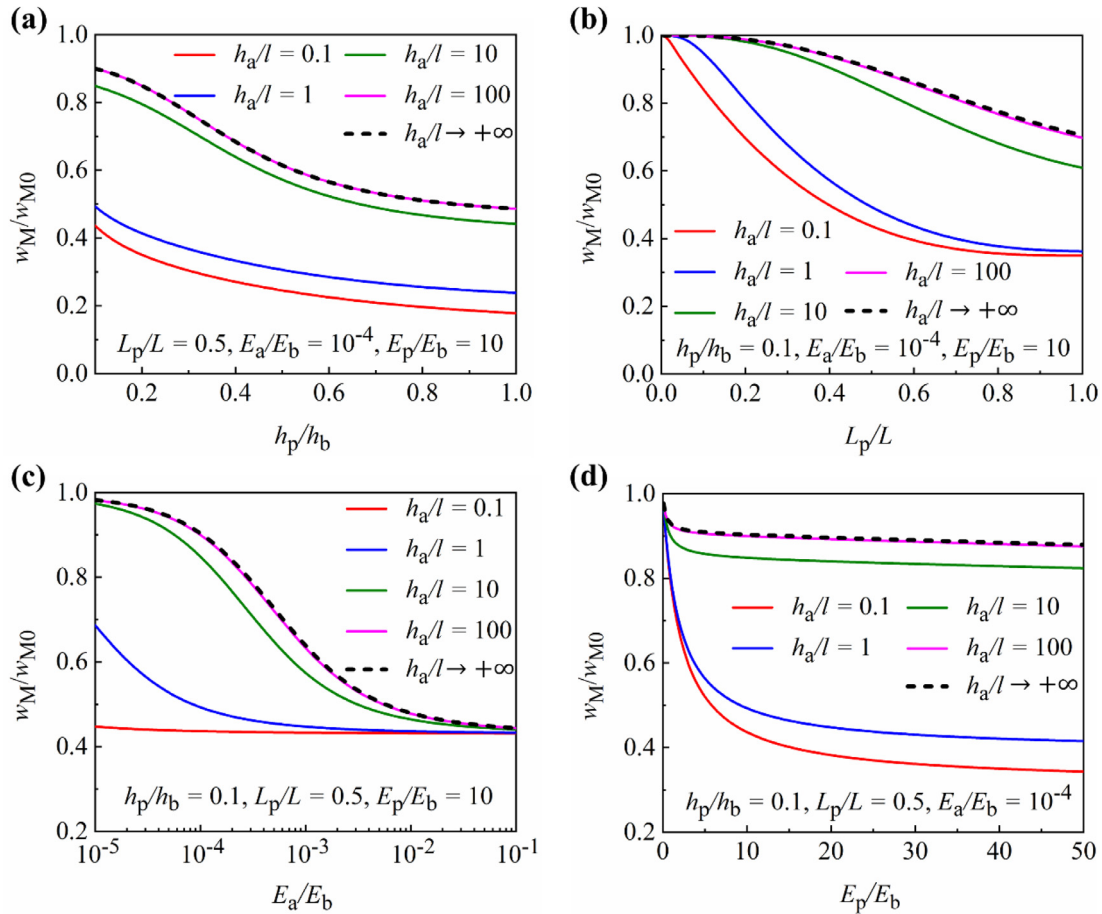
Fig. 6. For layered structures at different scales (represented by h_a/l), variations of the normalized midspan deflection of the host beam w_M/w_{M0} with the dimensionless (a) plate thickness h_p/h_b, (b) plate length L_p/L, (c) adhesive modulus E_a/E_b and (d) plate modulus E_p/E_b. The midspan deflection is normalized by $w_{M0} = L^3/(4E_b b h_b^3)$, the midspan deflection of the host beam without a bonded plate. For all curves, $h_a/h_b = 10^{-2}$, $L/h_b = 20$ and $v_a = 0.4$. The limiting case of $h_a/l \rightarrow +\infty$ (dashed curves) corresponds to the classical solution.

layer thickness varies from macro to micro scale). The geometry effects at the macro scale can be studied by the classical model, while the size effects should be captured by the present strain gradient model.

From Fig. 4, interfacial tractions tend to infinity near the plate end when $h_a/h_b \rightarrow 0$. And similar phenomenon can also be observed in Fig. 5 when $h_a/l \rightarrow 0$. On the one hand, these results are rigorous solutions to our analytical model. On the other hand, the traction singularity near the plate ends is not surprising if we consider the ends as the crack tip of the interface cracks (90° interface crack for host beam/adhesive interface and 180° interface crack for plate/adhesive interface). Actually, referring to the classical results about the stress singularities in bimaterial wedges [59], we can know that the interfacial stresses would have a power singularity at the plate ends if we treat the adherends and the adhesive layer as elastic continua. Generally, the 1D analysis based on the beam theory and adhesive layer theory cannot predict the stress singularities (i.e., interfacial stresses are bounded everywhere). However, interfacial stresses can tend to infinity near the plate ends when the adhesive layer thickness decreases to zero [29], due to infinity stiffnesses of the springs simplified from the adhesive layer (spring stiffnesses are inversely proportional to the adhesive layer thickness). Similarly, in the present strain gradient solution, as shown in Fig. 5, infinite interfacial tractions near the plate ends can be observed when $h_a/l \rightarrow 0$, indicating that the adhesive layer becomes very stiff owing to large strain gradients.

3.1.2. Midspan deflection of the host beam

Herein, the midspan deflection of the host beam in layered structures is denoted by $w_M = w_b(L_p/2)$, and the midspan deflection of the host

beam without a bonded plate is represented by w_{M0}. Due to the stiffening effects of the bonded plate on the host beam, which are transferred by the adhesive layer, the midspan deflection of the host beam becomes smaller for the same applied load, i.e., $w_M \leq w_{M0}$.

Fig. 6 plots the normalized midspan deflection w_M/w_{M0} for layered structures at different scales. Generally, these results correspond to the unbalanced case, and only a particular combination of the geometry and material parameters corresponds to the balanced case. For example, in Fig. 6(a), we can know that $\lambda_3 = 0$ (the balanced case) is satisfied only when $h_p/h_b \approx 0.32$ from Eq. (27b). From Fig. 6, if the stiffening effects of the plate can be neglected (e.g., $L_p/L \rightarrow 0$), w_M/w_{M0} tends to unity. And whatever the structure scale is, the midspan deflection decreases when the plate thickness, plate length, adhesive modulus and plate modulus increase, which indicates that the stiffening effects of the plate increases. Here, free boundary conditions at the adhesive ends are ignored, even for $L_p/L \rightarrow 1$. For large values of plate length, the size of the regions affected by the adhesive ends is much smaller than the plate length.

The variation of the normalized midspan deflection with the dimensionless plate thickness is presented in Fig. 6(a). In Fig. 6(a), when h_a/l decreases from infinity to 100, the strain gradient solution is almost the same as the classical solution, implying that the strain gradient effects can be ignored. However, when the structure scale further decreases (h_a/l decreases), the deflection exhibits an obvious size effect. As the adhesive layer thickness reaches the micron level ($h_a/l = 1$), the midspan deflection of the strain gradient solution decreases significantly compared with that of the classical solution, arising from the stiff interface bonding of the micro-scale adhesive layers due to large strain gradients.
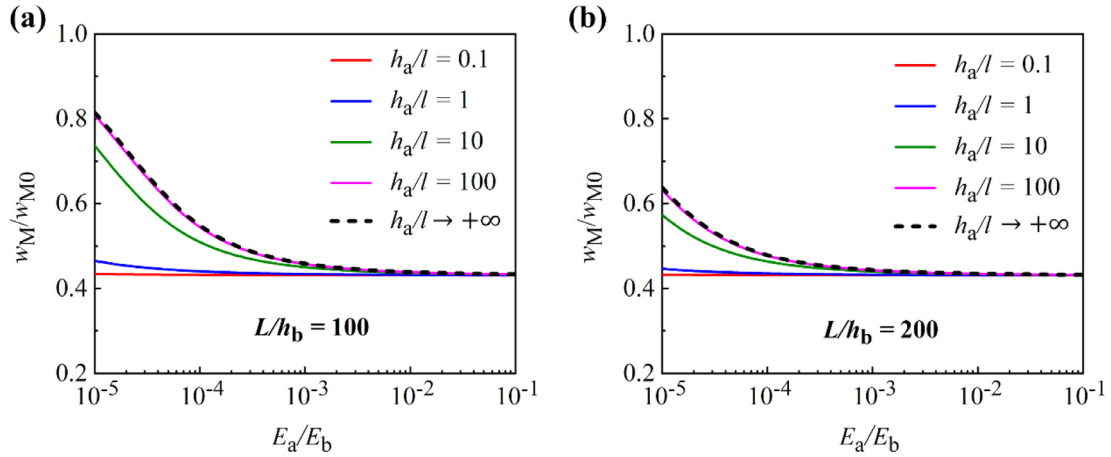
Fig. 7. For layered structures at different scales (represented by h_a/l), variations of the normalized midspan deflection of the host beam w_M/w_{M0} with the dimensionless adhesive modulus E_a/E_b for different dimensionless span lengths L/h_b: (a) $L/h_b = 100$ and (b) $L/h_b = 200$. For all curves, $h_a/h_b = 10^{-2}$, $h_p/h_b = 0.1$, $L_p/L = 0.5$, $v_a = 0.4$ and $E_p/E_b = 10$. The limiting case of $h_a/l \to +\infty$ (dashed curves) corresponds to the classical solution.

For $h_a/l = 0.1$, the midspan deflection further decreases. Similar trends can also be found in Fig. 6(b)–(d).

As illustrated in Fig. 6(c), the difference between the strain gradient solution and the classical solution is apparent when the adhesive modulus is small. Furthermore, it is worth noting that when the adhesive layer thickness is on the same order of magnitude as the material characteristic length scale or even smaller ($h_a/l \leq 1$), the midspan deflection is almost independent of the adhesive modulus in a wide range, due to the strong strain gradient effects. Therefore, the adhesive modulus becomes unimportant in this case. This phenomenon is quite different from the behavior of macro-scale layered structures, where the adhesive layer with low modulus leads to flexible bonding and the host beam deflection becomes larger (the dashed line in Fig. 6(c)). Therefore, we can use very soft micro-scale adhesive layers (with low modulus) to realize a stiff interface bonding, which is crucial to achieving excellent performance for micro devices, such as high accuracy and repeatability of signal detection.

The above discussions are aimed at layered structures with a span length (or aspect ratio of the host beam) of $L/h_b = 20$, similar to some previous studies [38,41,60]. For larger span lengths, which are common in flexible electronics [19,26], the variation of midspan deflection with adhesive modulus is shown in Fig. 7. Combining Fig. 6(c) with Fig. 7(a), (b), we can see that with the increase of span length, the difference between the classical solution and the strain gradient solution decreases. However, the trends in midspan deflection are similar. And even for $L/h_b = 200$ and $E_a/E_b = 10^{-5}$ (Fig. 7(b)), the deflection of the strain gradient solution ($h_a/l = 0.1$) can be 32% smaller than that of the classical solution.

3.2. Results of layered structures with micro-scale adhesive layers

In this section, we will focus on the case of $h_a/l = 1$, where the layered structures are at the micro scale (with micro-scale adhesives). Besides, the span length is fixed at $L/h_b = 20$ and the values of other parameters are similar to those in Section 3.1.

3.2.1. Distributions of interfacial tractions

For layered structures with micro-scale adhesive layers, influences of plate thickness on the distributions of interfacial tractions are presented in Fig. 8. It can be seen that with the increase of the plate thickness, the shear traction decreases while the normal traction increases in a wide region. From Fig. 8(b), when the plate thickness increases, the compression zone enlarges and the maximum compression traction increases.

Fig. 9 shows the influences of the plate length on the distributions of interfacial tractions. It can be seen that with the decrease of the plate

length, the shear and normal tractions increase in a wide region, since the bending moment near the plate end increases for shorter plates. From Fig. 9(b), for small plate length ($L_p/L = 0.2$), the interface is always under compression when $x/L_p > 0.1$, which can be explained by considering that the influence region of the plate end covers the whole interface. In contrast, for larger plate lengths ($L_p/L = 0.5$, 0.8), the influence region is limited to the vicinity of the plate end, and thus the normal traction decreases to zero quickly.

The influences of the adhesive modulus on the distributions of interfacial tractions are shown in Fig. 10. As the adhesive modulus increases, the interfacial shear and normal tractions increase substantially, indicating that the adhesive layers with larger modulus can ensure stiffer bonding between the plate and the host beam. For $E_a/E_b = 10^{-2}$, we can observe large compression traction (Fig. 10(b)).

Fig. 11 shows the influences of the plate modulus on the distributions of interfacial tractions. It can be found that with the increase of the plate modulus, the shear traction increases. From Fig. 11(b), when the plate modulus increases, the compression zone enlarges and the maximum compression traction increases.

From the discussions above, we can find that with the increase of adhesive modulus or the decrease of the plate length, the shear and normal tractions increase in a wide region of the interface. Since high interfacial tractions can cause interfacial delamination, the stress distribution combined with a suitable failure criterion can be used to predict the strength of adhesively bonded joints [1]. Therefore, the theoretical predictions of the interfacial tractions presented here can help the strength prediction and the optimal design of layered structures to avoid premature failure, particularly for layered structures with micro-scale adhesive layers.

3.2.2. Midspan deflection of the host beam

For layered structures with micro-scale adhesive layers ($h_a/l = 1$), influences of the plate geometry on the normalized midspan deflection of the host beam are presented in Fig. 12. From Fig. 12(a), the midspan deflection decreases as the plate thickness increases, because the bending stiffness of the plate $E_p b h_p^3/12$ increases. However, for short plate ($L_p/L = 0.2$), the variation of deflection is insensitive to the plate thickness. In this case, the bending stiffness of the short plate is large enough. Thus the plate almost acts like a rigid body and only small deformation occurs. Then, although the plate thickness is increased, its stiffening effect on the host beam cannot be further enhanced.

As shown in Fig. 12(b), with the increase of plate length, the midspan deflection decreases at first and eventually tends to be stable, indicating the saturation of the stiffening effects of the plate. This saturation phenomenon is related to the loading condition of three-point bend-
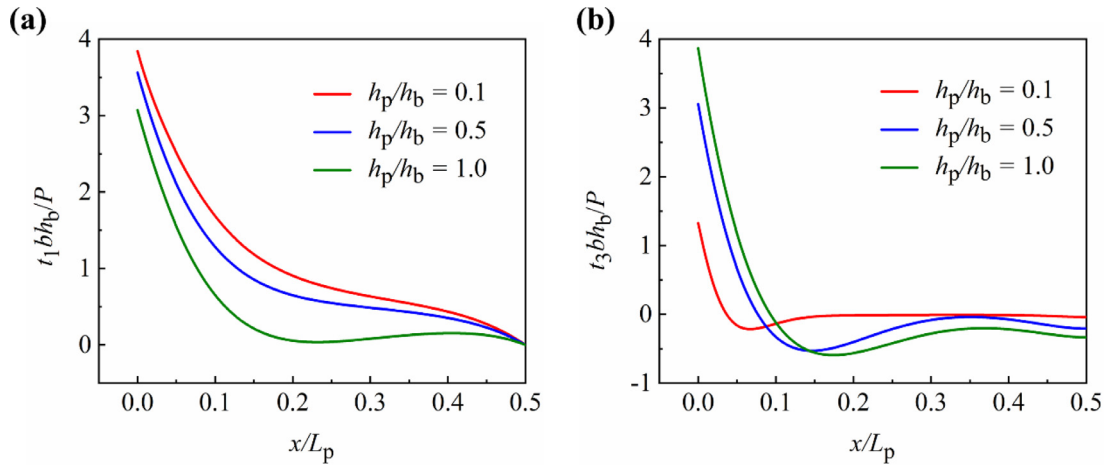
Fig. 8. Influences of the dimensionless plate thickness h_p/h_b on the distributions of interfacial tractions for layered structures with micro-scale adhesive layers ($h_a/l = 1$): dimensionless (a) interfacial shear traction $t_1 bh_b/P$ and (b) interfacial normal traction $t_3 bh_b/P$ versus normalized distance from the plate end x/L_p. The values of other parameters are fixed at $h_a/h_b = 10^{-2}$, $L_p/L = 0.5$, $L/h_b = 20$, $E_a/E_b = 10^{-4}$, $\nu_a = 0.4$ and $E_p/E_b = 10$.
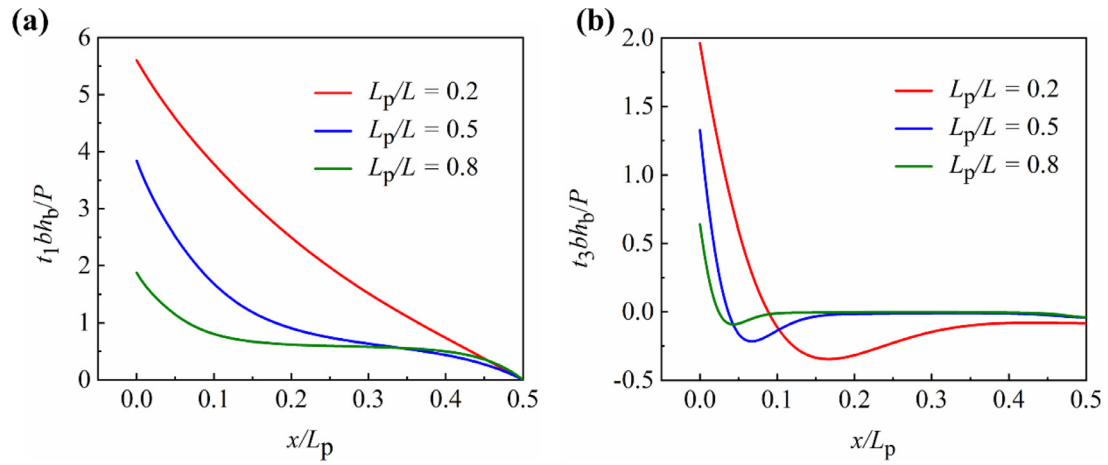
Fig. 9. Influences of the dimensionless plate length L_p/L on the distributions of interfacial tractions for layered structures with micro-scale adhesive layers ($h_a/l = 1$): dimensionless (a) interfacial shear traction $t_1 bh_b/P$ and (b) interfacial normal traction $t_3 bh_b/P$ versus normalized distance from the plate end x/L_p. The values of other parameters are fixed at $h_a/h_b = 10^{-2}$, $h_p/h_b = 0.1$, $L/h_b = 20$, $E_a/E_b = 10^{-4}$, $\nu_a = 0.4$ and $E_p/E_b = 10$.
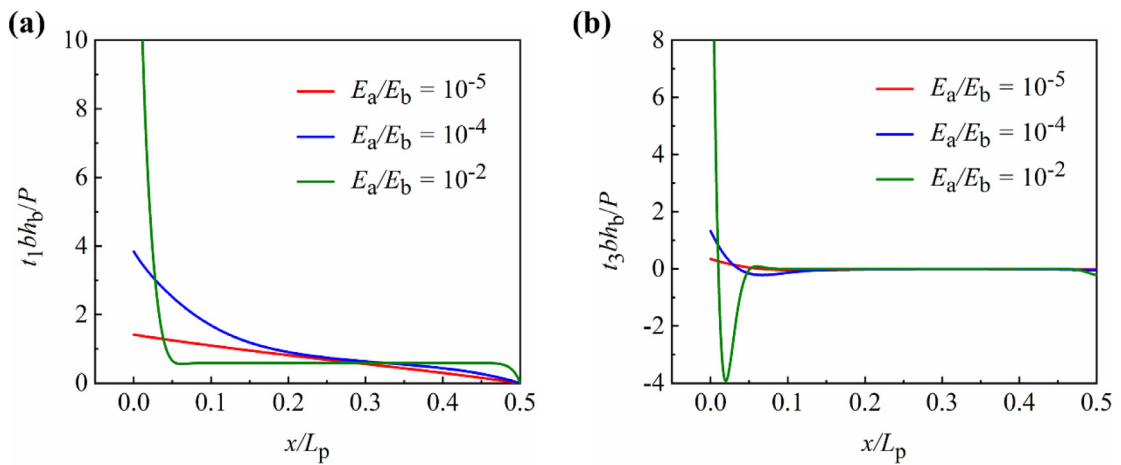
Fig. 10. Influences of the dimensionless adhesive modulus E_a/E_b on the distributions of interfacial tractions for layered structures with micro-scale adhesive layers ($h_a/l = 1$): dimensionless (a) interfacial shear traction $t_1 bh_b/P$ and (b) interfacial normal traction $t_3 bh_b/P$ versus normalized distance from the plate end x/L_p. The values of other parameters are fixed at $h_a/h_b = 10^{-2}$, $h_p/h_b = 0.1$, $L_p/L = 0.5$, $L/h_b = 20$, $\nu_a = 0.4$ and $E_p/E_b = 10$.
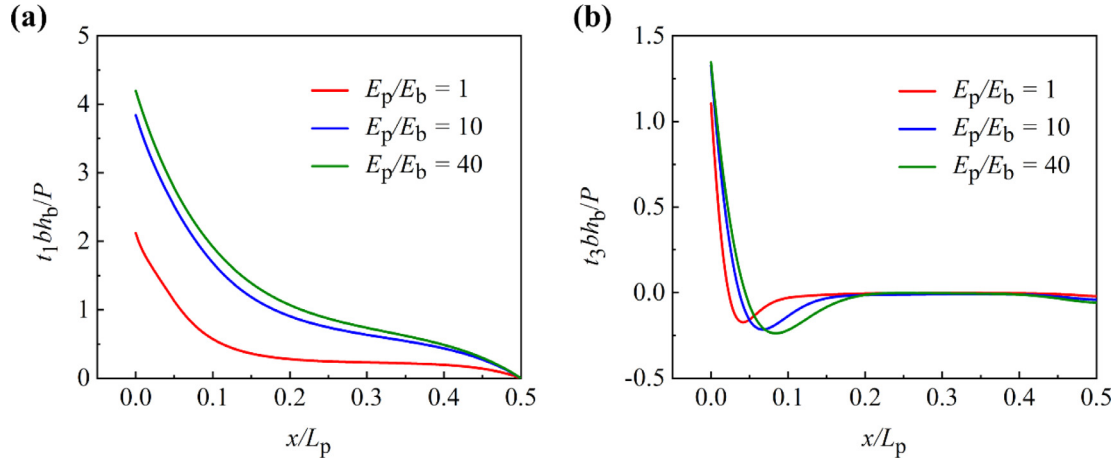
Fig. 11. Influences of the dimensionless plate modulus E_p/E_b on the distributions of interfacial tractions for layered structures with micro-scale adhesive layers ($h_a/l = 1$): dimensionless (a) interfacial shear traction $t_1 bh_b/P$ and (b) interfacial normal traction $t_3 bh_b/P$ versus normalized distance from the plate end x/L_p. The values of other parameters are fixed at $h_a/h_b = 10^{-2}$, $h_p/h_b = 0.1$, $L_p/L = 0.5$, $L/h_b = 20$, $E_a/E_b = 10^{-4}$ and $v_a = 0.4$.
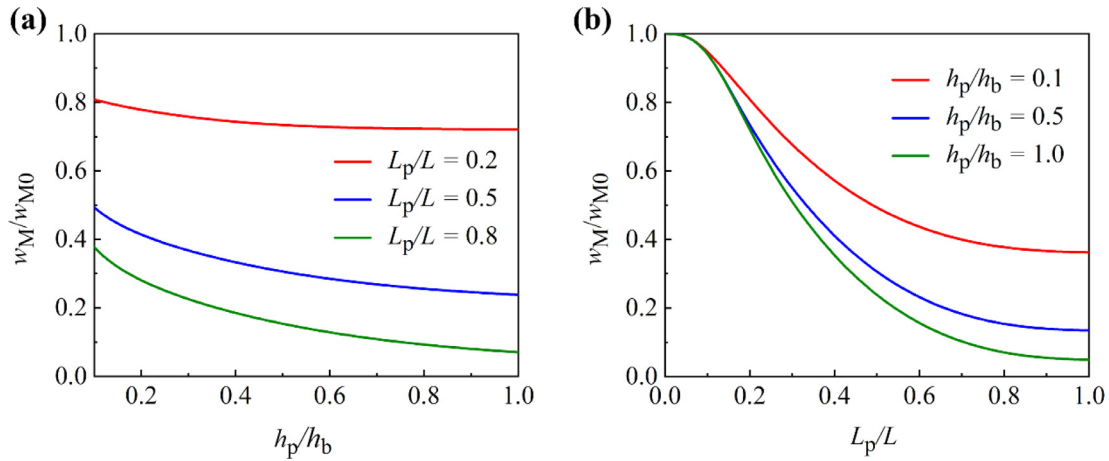
Fig. 12. Influences of the plate geometry on the normalized midspan deflection of the host beam w_M/w_{M0} for layered structures with micro-scale adhesive layers ($h_a/l = 1$): (a) w_M/w_{M0} versus dimensionless plate thickness h_p/h_b for different dimensionless plate lengths L_p/L; (b) w_M/w_{M0} versus L_p/L for different values of h_p/h_b. The values of other parameters are fixed at $h_a/h_b = 10^{-2}$, $L/h_b = 20$, $E_a/E_b = 10^{-4}$, $v_a = 0.4$ and $E_p/E_b = 10$.
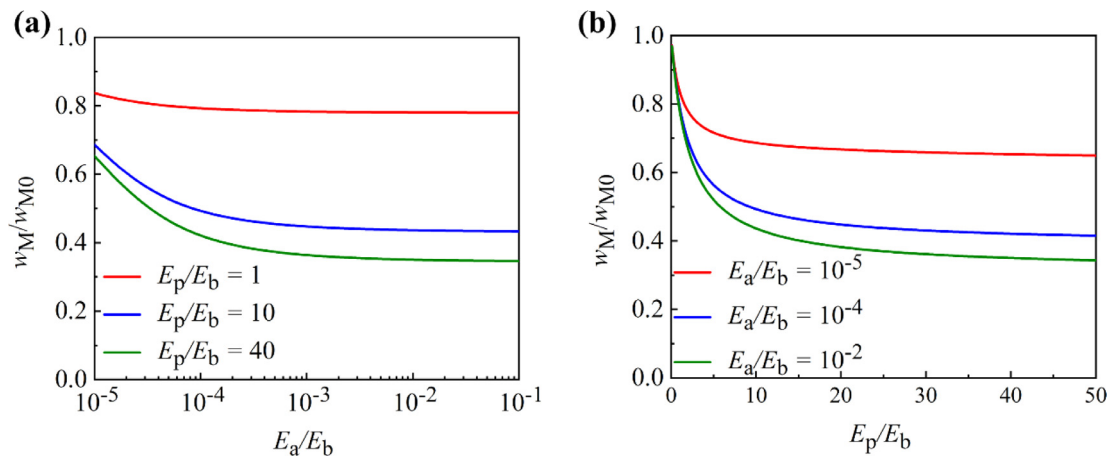
Fig. 13. Influences of the material properties on the normalized midspan deflection of the host beam w_M/w_{M0} for layered structures with micro-scale adhesive layers ($h_a/l = 1$): (a) w_M/w_{M0} versus dimensionless adhesive modulus E_a/E_b for different dimensionless plate moduli E_p/E_b; (b) w_M/w_{M0} versus E_p/E_b for different values of E_a/E_b. The values of other parameters are fixed at $h_a/h_b = 10^{-2}$, $h_p/h_b = 0.1$, $L_p/L = 0.5$, $L/h_b = 20$ and $v_a = 0.4$.

ing. With the increase of the distance from the midspan, the bending moment decreases, and thus the influence of increasing plate length becomes weaker. If we want to minimize the deflection of the host beam, it is economical and efficient to use a plate with the critical length, which corresponds to the saturation of the stiffening effects.

Fig. 13 shows the influences of the material properties on the normalized midspan deflection of the host beam. In Fig. 13(a), the deflection almost remains constant for a wide range of adhesive moduli, which is attributed to the strong strain gradient effects in the constrained microscale adhesives, as discussed in Section 3.1.2. This phenomenon is similar for different plate moduli. From Fig. 13(b), when the plate modulus increases, the midspan deflection of the host beam decreases dramatically within the range of $E_p/E_b < 5$. Afterwards, the deflection reaches a plateau, indicating that the large bending stiffness of the plate leads to the saturation of its stiffening effects on the host beam.

4. Conclusions

In summary, a size-dependent model for predicting the mechanical behaviors of adhesively bonded layered structures is established. The thin adhesive layer is characterized by the strain gradient elasticity while the adherends, including the host beam and the bonded plate, are described by the classical Euler-Bernoulli beam theory. The main conclusions are summarized as follows:

(1) The proposed analytical model can predict the size effects of the mechanical behaviors of adhesively bonded layered structures. When the structure scale decreases (the adhesive layer thickness also decreases), the interfacial tractions increase substantially and the midspan deflection of the host beam decreases significantly, especially for soft adhesive layers with low modulus. Although the predicted interfacial tractions near the adhesive ends are inaccurate, they are valid for the locations a little far away from the adhesive ends.

(2) When the adhesive layer thickness is comparable to its material characteristic length scale (on the order of microns), the host beam deflection is insensitive to the adhesive modulus, indicating the stiff bonding due to the large strain gradients in the constrained micro-scale adhesive layer.

(3) For layered structures with micro-scale adhesive layers, when the adhesive modulus increases or the plate length decreases, the shear and normal tractions increase in a wide region of the interface. With the increase of the plate thickness, plate length and plate modulus, the midspan deflection decreases firstly and then tends to saturate, corresponding to the saturation of stiffening effects of the boned plate on the host beam.

Declaration of Competing Interest

The authors declare that they have no known competing financial interests or personal relationships that could have appeared to influence the work reported in this paper.

CRediT authorship contribution statement

Hao Long: Formal analysis, Methodology, Writing - original draft. **Hansong Ma:** Methodology, Writing - review & editing. **Yueguang Wei:** Conceptualization, Funding acquisition, Resources, Supervision, Writing - review & editing. **Yanwei Liu:** Formal analysis, Methodology.

Acknowledgments

Appendix A. Expressions of the coefficients in Eqs. (19)

A.1. The general case

The expressions of a_{ij} in Eq. (19a) are given by

$$a_{11} = -\frac{\cosh \bar{A} - 1}{K_1}, \; a_{21} = -\frac{\sinh \bar{A}}{K_1}, \; a_{31} = -\frac{\bar{A} \sinh \bar{A}}{K_1}, \tag{A.1}$$

where

$$K_1 = \bar{A}\sinh\bar{A} - 2\cosh\bar{A} + 2 > K_1(\bar{A} = 0) = 0. \tag{A.2}$$

The expressions of a_{ij} in Eq. (19b) are given by

$$a_{51} = -\frac{\cosh \bar{B} - 1}{K_2}, \tag{A.3a}$$

$$a_{53} = \frac{(\cosh\bar{B} - 1)}{K_2}(b_3 - b_1 - b_5) + \frac{(\bar{B} - \sinh\bar{B})}{\bar{B}K_2}(b_7 - b_5), \tag{A.3b}$$

$$a_{54} = \frac{(\cosh\bar{B} - 1)}{K_2}(b_4 - b_2 - b_6) + \frac{(\bar{B} - \sinh\bar{B})}{\bar{B}K_2}(b_8 - b_6), \tag{A.3c}$$

$$a_{61} = \frac{\sinh \bar{B}}{K_2}, \tag{A.3d}$$

$$a_{63} = -\frac{\sinh \bar{B}}{K_2}(b_3 - b_1 - b_5) + \frac{(\cosh\bar{B} - 1)}{\bar{B}K_2}(b_7 - b_5), \tag{A.3e}$$

$$a_{64} = -\frac{\sinh \bar{B}}{K_2}(b_4 - b_2 - b_6) + \frac{(\cosh\bar{B} - 1)}{\bar{B}K_2}(b_8 - b_6), \tag{A.3f}$$

$$a_{71} = -\frac{\bar{B} \sinh \bar{B}}{K_2}, \tag{A.3g}$$

$$a_{73} = \frac{\bar{B} \sinh \bar{B}}{K_2}(b_3 - b_1) - \frac{(\cosh\bar{B} - 1)}{K_2}(b_7 + b_5), \tag{A.3h}$$

$$a_{74} = \frac{\bar{B} \sinh \bar{B}}{K_2}(b_4 - b_2) - \frac{(\cosh\bar{B} - 1)}{K_2}(b_8 + b_6), \tag{A.3i}$$

$$a_{83} = b_1 - a_{53}, \; a_{84} = b_2 - a_{54}, \tag{A.3j}$$

where

$$K_2 = \bar{B}\sinh\bar{B} - 2\cosh\bar{B} + 2 > K_2(\bar{B} = 0) = 0, \tag{A.4}$$

$$b_1 = -\frac{1}{2} - b_2, \; b_2 = \frac{\bar{B}^2\bar{h}_a}{(\bar{A}^2 - \bar{B}^2)\bar{A}}a_{21}, \tag{A.5a}$$

$$b_3 = \frac{\bar{h}_a}{2}a_{31} - b_2, \; b_4 = \frac{\bar{h}_p}{2} - b_3, \tag{A.5b}$$

$$b_5 = -\bar{h}_a - b_6, \; b_6 = \frac{\bar{B}^2\bar{h}_a}{\bar{A}^2 - \bar{B}^2}a_{11}, \tag{A.5c}$$

$$b_7 = \bar{h}_a a_{31} + b_6, \; b_8 = -\bar{h}_a - b_7. \tag{A.5d}$$

A.2. Two limit cases

For $h_a/l \to +\infty$, the expressions of a_{ij} degenerate into those of classical solution. From Eqs. (A.1)–(A.5), we can obtain

$$a_{31} \to -1, \ a_{71} \to -1, \ a_{73} \to \frac{1 - \bar{h}_a}{2}, \ a_{74} \to \frac{\bar{h}_p + \bar{h}_a}{2}, \ a_{83} \to -\frac{1}{2}. \quad (A.6)$$

Other coefficients a_{ij} tend to zero. Therefore, interfacial tractions of the classical solution can be obtained from Eqs. (20):

$$\bar{t}_1 \to \frac{\bar{G}_a}{\bar{h}_a}\left(\bar{u}_{p0} - \bar{u}_{b0} + \frac{1 + \bar{h}_a}{2}\frac{d\bar{w}_b}{d\bar{x}} + \frac{\bar{h}_p + \bar{h}_a}{2}\frac{d\bar{w}_p}{d\bar{x}}\right), \ \bar{t}_3 \to \frac{\bar{E}_a}{\bar{h}_a}(\bar{w}_p - \bar{w}_b). \quad (A.7)$$

For $h_a/l \to 0^+$, the strain gradient effects cannot be enhanced anymore. From Eqs. (A.1)–(A.5), we can find $a_{ij} \to \infty$, and thus numerical singularities are encountered. However, some relations can be obtained by the following analysis. According to Eqs. (19), we have

$$C_1 = a_{11}(\bar{w}_b - \bar{w}_p), \ C_5 = a_{51}\left(\bar{u}_{b0} - \bar{u}_{p0} + \frac{a_{53}}{a_{51}}\frac{d\bar{w}_b}{d\bar{x}} + \frac{a_{54}}{a_{51}}\frac{d\bar{w}_p}{d\bar{x}}\right). \quad (A.8)$$

Since the coefficient C_1 and C_5 are finite, combining Eq. (A.8) with Eqs. (A.3a)–(A.3c) and (16), we can obtain

$$\bar{w}_b - \bar{w}_p \to 0, \ \bar{u}_b(\bar{z} = 0) - \bar{u}_p(\bar{z} = 1) \to \bar{h}_a\frac{d\bar{w}_b}{d\bar{x}}. \quad (A.9)$$

If $\bar{h}_a \to 0$, the displacements of the lower surface of the host beam and those of the upper surface of the bonded plate are equal. This case can be called 'perfect bonding'.

Appendix B. Roots of the characteristic equation of Eq. (42)

The characteristic equation of Eq. (42) can be expressed by

$$(\eta^6 - \alpha_1\eta^4 + \alpha_2\eta^2 - \alpha_3)\eta^3 = 0. \quad (B.1)$$

Thus, $\eta = 0$ or the expression in the parentheses is zero, i.e.,

$$\zeta^3 + 3\beta_1\zeta - 2\beta_2 = 0, \quad (B.2)$$

where $\zeta = \eta^2 - \alpha_1/3$ and

$$\beta_1 = \frac{3\alpha_2 - \alpha_1^2}{9}, \ \beta_2 = \frac{2\alpha_1^3 - 9\alpha_1\alpha_2 + 27\alpha_3}{54}. \quad (B.3)$$

For typical material and geometry parameters, the discriminant $\Delta = \beta_1^3 + \beta_2^2 > 0$, and thus Eq. (B.2) has one real root and two non-real complex conjugate roots:

$$\zeta_1 = \beta_3, \ \zeta_{2,3} = -\frac{1}{2}\beta_3 \pm \frac{\sqrt{3}}{2}\beta_4 i, \quad (B.4)$$

where $i = \sqrt{-1}$ and

$$\beta_{3,4} = \sqrt[3]{\beta_2 + \sqrt{\Delta}} \pm \sqrt[3]{\beta_2 - \sqrt{\Delta}}. \quad (B.5)$$

Generally, we have $\alpha_1/3 + \beta_3 > 0$. Then, Eq. (B.1) has two nonzero real roots, two pairs of conjugate complex roots and three zero roots:

$$\eta_{1,2} = \pm\sqrt{\frac{\alpha_1}{3} + \beta_3}, \ \eta_{3,4} = \gamma_1 \pm \gamma_2 i, \ \eta_{5,6} = -\gamma_1 \pm \gamma_2 i, \ \eta_{7,8,9} = 0, \quad (B.6)$$

where β_5 and β_6 are positive parameters defined as

$$\gamma_{1,2} = \sqrt{\frac{1}{2}\left[\sqrt{\left(\frac{\alpha_1}{3} - \frac{\beta_3}{2}\right)^2 + \frac{3\beta_4^2}{4}} \pm \left(\frac{\alpha_1}{3} - \frac{\beta_3}{2}\right)\right]}. \quad (B.7)$$

Appendix C. An approximate solution for small thickness ratios of adhesive layer to adherends

Based on the complete shear strain expression in Eq. (10a), a rigorous analysis is presented in the main text. If we ignore the term $\partial w_a/\partial x$ in Eq. (10a), we can obtain an approximate solution following the analysis in Sections 2.2 and 2.3. As a result, the adhesive displacement $\bar{w}_a$ is still expressed by Eq. (18a) while $\bar{u}_a$ is given by

$$\bar{u}_a^* = C_5\cosh(\bar{B}\bar{z}) + C_6\sinh(\bar{B}\bar{z}) + C_7\bar{z} + C_8. \quad (C.1)$$

The integration constants C_i ($i = 1$–8) can be expressed by Eqs. (19), and Eqs. (A.1), (A.2), (A.3a), (A.3d), (A.3g) and (A.4) are still valid. However, the coefficients a_{ij} ($i = 5$–8, $j = 3, \ 4$) should be replaced by

$$a_{53}^* = \frac{(\cosh\bar{B} - 1)}{2K_2}(1 + 2\bar{h}_a) + \frac{(\bar{B} - \sinh\bar{B})}{\bar{B}K_2}\bar{h}_a, \quad (C.2a)$$

$$a_{54}^* = \frac{(\cosh\bar{B} - 1)}{2K_2}\bar{h}_p - \frac{(\bar{B} - \sinh\bar{B})}{\bar{B}K_2}\bar{h}_a, \quad (C.2b)$$

$$a_{63}^* = -\frac{\sinh\bar{B}}{2K_2}(1 + 2\bar{h}_a) + \frac{(\cosh\bar{B} - 1)}{\bar{B}K_2}\bar{h}_a, \quad (C.2c)$$

$$a_{64}^* = -\frac{\sinh\bar{B}}{2K_2}\bar{h}_p - \frac{(\cosh\bar{B} - 1)}{\bar{B}K_2}\bar{h}_a, \quad (C.2d)$$

$$a_{73}^* = \frac{\bar{B}\sinh\bar{B}}{2K_2} - \frac{(\cosh\bar{B} - 1)}{K_2}\bar{h}_a, \quad (C.2e)$$

$$a_{74}^* = \frac{\bar{B}\sinh\bar{B}}{2K_2}\bar{h}_p + \frac{(\cosh\bar{B} - 1)}{K_2}\bar{h}_a, \quad (C.2f)$$
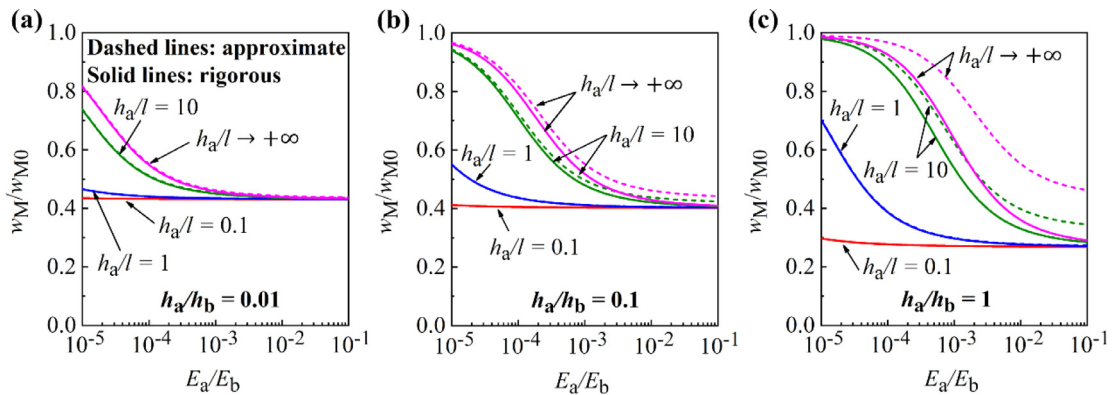
Fig. C.1. For layered structures at different scales (represented by h_a/l), variations of the normalized midspan deflection of the host beam w_M/w_{M0} with the dimensionless adhesive modulus E_a/E_b for different values of h_a/h_b: (a) $h_a/h_b = 0.01$, (b)$h_a/h_b = 0.1$ and (c) $h_a/h_b = 1.0$. For all curves, $h_p/h_b = 0.1$, $L_p/L = 0.5$, $L/h_b = 100$, $\nu_a = 0.4$ and $E_p/E_b = 10$. The dashed lines correspond to the approximate solution while the solid lines correspond to the rigorous solution. The approximate solutions for $h_a/l \to +\infty$ refer to the classical solution of Long et al. [29].

$$a_{83}^* = -\frac{1}{2} - a_{53}^*, \ a_{84}^* = -a_{53}^*. \tag{C.2g}$$

Interfacial tractions are still expressed by Eqs. (20), but $\xi_1 = a_{73}^*$ and $\xi_2 = a_{74}^*$.

From Eqs. (A.3) and (C.2), we can find that $a_{ij}^* - a_{ij} = \mathrm{O}(\bar{h}_a)$. Then, we can know that $\bar{u}_a^* - \bar{u}_a = \mathrm{O}(\bar{h}_a)$ from Eqs. (18b) and (C.1). Thus, the difference between the rigorous solution and the approximate solution is approximately on the order of $\bar{h}_a$. If $h_a \ll h_b, h_p$, we can neglect the term $\partial w_a / \partial x$ in Eq. (10a). However, the adhesive layer thickness can be comparable to the adherend thickness in some micro devices such as flexible electronics [10,26]. The comparisons between the global displacements of the two solutions are presented in Fig. C.1. With the increase of h_a/h_b, h_a/l and E_a/E_b, the approximate solution deviates more significantly from the rigorous solution.

References

[1] Ramalho LDC, Campilho R, Belinha J, da Silva LFM. Static strength prediction of adhesive joints: a review. Int J Adhes Adhes 2020;96:102451.

[2] Xu Y, Wang S-K, Yao P, Wang Y, Chen D. An air-plasma enhanced low-temperature wafer bonding method using high-concentration water glass adhesive layer. Appl Surf Sci 2020;500:144007.

[3] Han L, Wang XD, Sun Y. The effect of bonding layer properties on the dynamic behaviour of surface-bonded piezoelectric sensors. Int J Solids Struct 2008;45(21):5599–612.

[4] Na WS, Baek J. A review of the piezoelectric electromechanical impedance based structural health monitoring technique for engineering structures. Sensors 2018;18(5):1307.

[5] Jin C, Wang X. Analytical modelling of the electromechanical behaviour of surface-bonded piezoelectric actuators including the adhesive layer. Eng Fract Mech 2011;78(13):2547–62.

[6] Ji B, Xie Z, Hong W, Jiang C, Guo Z, Wang L, et al. Stretchable Parylene-C electrodes enabled by serpentine structures on arbitrary elastomers by silicone rubber adhesive. J Materiomics 2020;6(2):330–8.

[7] Liu P, Liu J, Zhu X, Wu C, Liu Y, Pan W, et al. A highly adhesive flexible strain sensor based on ultra-violet adhesive filled by graphene and carbon black for wearable monitoring. Compos Sci Technol 2019;182:107771.

[8] Bleiker SJ, Visser Taklo MM, Lietaer N, Vogl A, Bakke T, Niklaus F. Cost-efficient wafer-level capping for mems and imaging sensors by adhesive wafer bonding. Micromachines 2016;7(10):192.

[9] Ha S, Chang F-K. Adhesive interface layer effects in PZT-induced Lamb wave propagation. Smart Mater Struct 2010;19(2):025006.

[10] Kim D-H, Kim Y-S, Wu J, Liu Z, Song J, Kim H-S, et al. Ultrathin silicon circuits with strain-isolation layers and mesh layouts for high-performance electronics on fabric, vinyl, leather, and paper. Adv Mater 2009;21(36):3703–7.

[11] Huesgen T, Lenk G, Albrecht B, Vulto P, Lemke T, Woias P. Optimization and characterization of wafer-level adhesive bonding with patterned dry-film photoresist for 3D MEMS integration. Sens Actuator A-Phys 2010;162(1):137–44.

[12] Ji G, Ouyang Z, Li G, Ibekwe S, Pang S-S. Effects of adhesive thickness on global and local Mode-I interfacial fracture of bonded joints. Int J Solids Struct 2010;47(18-19):2445–58.

[13] Li J, Liang L, Liu X, Ma H, Song J, Wei Y. Experimental studies on strengthening and failure mechanism for the metal/silicone rubber/metal bonding system. Int J Appl Mech 2018;10(3):1850029.

[14] Campilho R, Moura DC, Banea MD, da Silva LFM. Adhesive thickness effects of a ductile adhesive by optical measurement techniques. Int J Adhes Adhes 2015;57:125–32.

[15] Marzi S, Biel A, Stigh U. On experimental methods to investigate the effect of layer thickness on the fracture behavior of adhesively bonded joints. Int J Adhes Adhes 2011;31(8):840–50.

[16] Yang S, Xu W, Liang L, Wang T, Wei Y. An experimental study on the dependence of the strength of adhesively bonded joints with thickness and mechanical properties of the adhesives. J Adhes Sci Technol 2014;28(11):1055–71.

[17] Dagdeviren C, Yang BD, Su Y, Tran PL, Joe P, Anderson E, et al. Conformal piezoelectric energy harvesting and storage from motions of the heart, lung, and diaphragm. Proc Natl Acad Sci U S A 2014;111(5):1927–32.

[18] Wang Y, Qiu Y, Ameri SK, Jang H, Dai Z, Huang Y, et al. Low-cost, μm-thick, tape-free electronic tattoo sensors with minimized motion and sweat artifacts. NPJ Flex Electron 2018;2:6.

[19] Park S-I, Ahn J-H, Feng X, Wang S, Huang Y, Rogers JA. Theoretical and experimental studies of bending of inorganic electronic materials on plastic substrates. Adv Funct Mater 2008;18(18):2673–84.

[20] Bleiker SJ, Dubois V, Schröder S, Stemme G, Niklaus F. Adhesive wafer bonding with ultra-thin intermediate polymer layers. Sens Actuator A-Phys 2017;260:16–23.

[21] Fleck NA, Muller GM, Ashby MF, Hutchinson JW. Strain gradient plasticity: theory and experiment. Acta Metall Mater 1994;42(2):475–87.

[22] Liu D, He Y, Dunstan DJ, Zhang B, Gan Z, Hu P, et al. Toward a further understanding of size effects in the torsion of thin metal wires: an experimental and theoretical assessment. Int J Plast 2013;41:30–52.

[23] McFarland AW, Colton JS. Role of material microstructure in plate stiffness with relevance to microcantilever sensors. J Micromech Microeng 2005;15(5):1060–7.

[24] Lam DCC, Yang F, Chong ACM, Wang J, Tong P. Experiments and theory in strain gradient elasticity. J Mech Phys Solids 2003;51(8):1477–508.

[25] Chong ACM, Lam DCC. Strain gradient plasticity effect in indentation hardness of polymers. J Mater Res 1999;14(10):4103–10.

[26] Li S, Liu X, Li R, Su Y. Shear deformation dominates in the soft adhesive layers of the laminated structure of flexible electronics. Int J Solids Struct 2017;305–14;110-111:.

[27] Crawley EF, de Luis J. Use of piezoelectric actuators as elements of intelligent structures. AIAA J 1987;25(10):1373–85.

[28] Goland M, Reissner E. The stresses in cemented joints. J Appl Mech 1944;66:17–27.

[29] Long H, Wei Y, Liang L. A rigorous analytical solution of interfacial stresses and overall stiffness of beam structures bonded with partially covered plates. Int J Mech Sci 2020;167:105284.

[30] Jiang ZQ, Huang Y, Chandra A. Thermal stresses in layered electronic assemblies. J Electron Packag 1997;119:127–32.

[31] Toupin R. Elastic materials with couple-stresses. Arch Ration Mech Anal 1962;11:385–414.

[32] Mindlin RD, Tiersten HF. Effects of couple-stresses in linear elasticity. Arch Ration Mech Anal 1962;11(1):415–48.

[33] Yang F, Chong ACM, Lam DCC, Tong P. Couple stress based strain gradient theory for elasticity. Int J Solids Struct 2002;39(10):2731–43.

[34] Altan BS, Aifantis EC. On some aspects in the special theory of gradient elasticity. J Mech Behav Mater 1997;8(3):231–82.

[35] Mindlin RD. Micro-structure in linear elasticity. Arch Ration Mech Anal 1964;16(1):51–78.

[36] Zhou S, Li A, Wang B. A reformulation of constitutive relations in the strain gradient elasticity theory for isotropic materials. Int J Solids Struct 2016;80:28–37.

[37] Yang W, He D, Chen W. A size-dependent zigzag model for composite laminated micro beams based on a modified couple stress theory. Compos Struct 2017;179:646–54.

[38] Sidhardh S, Ray MC. Exact solution for size-dependent elastic response in laminated beams considering generalized first strain gradient elasticity. Compos Struct 2018;204:31–42.

[39] Khaje khabaz M, Eftekhari SA, Hashemian M, Toghraie D. Optimal vibration control of multi-layer micro-beams actuated by piezoelectric layer based on modified couple stress and surface stress elasticity theories. Physica A 2020;546:123998.

[40] Nikpourian A, Ghazavi MR, Azizi S. Size-dependent nonlinear behavior of a piezoelectrically actuated capacitive bistable microstructure. Int J Non-Linear Mech 2019;114:49–61.

[41] Fu G, Zhou S, Qi L. The size-dependent static bending of a partially covered laminated microbeam. Int J Mech Sci 2019;152:411–19.

[42] Ascione F. Adhesive lap-joints: a micro-scale numerical investigation. Mech Res Commun 2010;37(2):169–72.

[43] Agrawal BN, Treanor KE. Shape control of a beam using piezoelectric actuators. Smart Mater Struct 1999;8(6):729–39.

[44] Wei Y, Hutchinson JW. Steady-state crack growth and work of fracture for solids characterized by strain gradient plasticity. J Mech Phys Solids 1997;45(8):1253–73.

[45] Song J, Liu J, Ma H, Liang L, Wei Y. Determinations of both length scale and surface elastic parameters for fcc metals. C R Mecanique 2014;342(5):315–25.

[46] Wei Y. A new finite element method for strain gradient theories and applications to fracture analyses. Eur J Mech A-Solids 2006;25(6):897–913.

[47] Fleck NA, Hutchinson JW. Strain gradient plasticity. Adv Appl Mech 1997;33:295–361.

[48] Andersson T, Stigh U. The stress–elongation relation for an adhesive layer loaded in peel using equilibrium of energetic forces. Int J Solids Struct 2004;41(2):413–34.

[49] Ojalvo IU, Eidinoff HL. Bond thickness effects upon stresses in single-lap adhesive joints. AIAA J 1978;16(3):204–11.

[50] Ma H, Wei Y, Song J, Liang L. Mechanical behavior and size effect of the staggered bio-structure materials. Mech Mater 2018;126:47–56.

[51] Teng JG, Zhang JW, Smith ST. Interfacial stresses in reinforced concrete beams bonded with a soffit plate: a finite element study. Constr Build Mater 2002;16(1):1–14.

[52] Smith ST, Teng JG. Interfacial stresses in plated beams. Eng Struct 2001;23(7):857–71.

[53] Niiranen J, Khakalo S, Balobanov V, Niemi AH. Variational formulation and isogeometric analysis for fourth-order boundary value problems of gradient-elastic bar and plane strain/stress problems. Comput Meth Appl Mech Eng 2016;308:182–211.

[54] Niiranen J, Balobanov V, Kiendl J, Hosseini SB. Variational formulations, model comparisons and numerical methods for Euler–Bernoulli micro- and nano-beam models. Math Mech Solids 2019;24(1):312–35.

[55] Liu Z, Huang Y, Yin Z, Bennati S, Valvo PS. A general solution for the two-dimensional stress analysis of balanced and unbalanced adhesively bonded joints. Int J Adhes Adhes 2014;54:112–23.

[56] Luo QT, Tong LY. Exact static solutions to piezoelectric smart beams including peel stresses. II. Numerical results, comparison and discussion. Int J Solids Struct 2002;39(18):4697–722.

[57] Su Y, Li S, Li R, Dagdeviren C. Splitting of neutral mechanical plane of conformal, multilayer piezoelectric mechanical energy harvester. Appl Phys Lett 2015;107(4):041905.

[58] Song J, Fan C, Ma H, Wei Y. Hierarchical structure observation and nanoindentation size effect characterization for a limnetic shell. Acta Mech Sin 2015;31(3):364–72.

[59] Hein VL, Erdogan F. Stress singularities in a two-material wedge. Int J Fract Mech 1971;7:317–30.

[60] Kong S, Zhou S, Nie Z, Wang K. Static and dynamic analysis of micro beams based on strain gradient elasticity theory. Int J Eng Sci 2009;47(4):487–98.